238
3-26-79

DR 2373

SAND77-1681
Unlimited Release
UC-79c

PREDICTION OF THERMAL CAPABILITY FOR A PROPOSED LMFBR SPENT FUEL SHIPPING CASK

A. W. REED

SF 2900 Q(7-73)

SAND77-1681

PREDICTION OF THERMAL CAPABILITY FOR A PROPOSED LMFBR SPENT FUEL SHIPPING CASK

A. W. Reed
Fluid Mechanics & Heat Transfer Division 5511
Sandia Laboratories
Albuquerque, NM 87185

February 1979

ABSTRACT

Prediction of the thermal capability of a fast breeder spent fuel shipping cask requires consideration of a large number of variables, such as geometry, canister packing fluid, gaseous coolant pressure, surface emissivities and fin densities. In order to evaluate the individual influences of the large number of controlling parameters, a parametric analysis of a conceptual cask has been performed. Results of the analysis are applied to four options, each having a different configuration. Comparison of the options indicates that substantial increases in cask thermal capability may be obtained by the use of liquid sodium as a primary coolant and aluminum as a basket material.

TABLE OF CONTENTS

LIST OF FIGURES

LIST OF FIGURES (cont)

LIST OF TABLES

NOMENCLATURE

A	Area
D	Diameter
$\mathcal{F}$	Radiative configuration factor
g	Gravitational constant
h	Heat transfer coefficient
k	Thermal conductivity
L	Length
M	Molecular weight
n	Linear fin density
N	Number of assemblies in cask
Nu	Nusselt number
P	Pressure
Per	Perimeter (length)
Pr	Prandtl number
Q	Axial power density of fuel pin assembly
Q_{sol}	Solar flux
r	Radius
Ra	Rayleigh number
t	Thickness
T	Temperature

Greek Letters

α	Absorptivity
α_v	Absorptivity in the visible spectrum
α_{ve}	Effective absorptivity in the visible spectrum

NOMENCLATURE (cont)

β	Coefficient of thermal expansion
δ	Gap thickness
Δ	Difference between values
ε	Emissivity
ε_e	Effective emissivity
η_f	Fin efficiency
ν	Kinematic viscosity
σ	Stefan-Boltzmann constant

INTRODUCTION

A spent fuel shipping cask technology program is underway at Sandia Laboratories to assist in meeting the shipping needs of the United States Breeder Reactor program (BRP). The initial efforts of this program, which is funded by the Department of Energy/Reactor Research and Technology (formerly ERDA/RDD), have led to a series of conceptual designs for the shipping casks.[2] These concepts differ, to a great extent, in the manner by which decay heat is transferred from the fuel assemblies to the environment during both normal shipping and loading.

A spent fuel shipping cask performs two functions. First, it shields surrounding personnel from the harmful levels of radiation produced by the spent fuel. Secondly, it insures the containment of the spent fuel so that it can be transported and handled in a safe manner. It must perform both functions under normal and accident conditions.

When designing a cask, thermal effects must be considered. If fuel pins become too hot, a number of undesirable events may occur such as fuel or clad failure and fission gas release. For this reason, current guidelines[1] require that fuel pins not exceed a temperature of 538°C (1000°F) while the cask rests in still air with a temperature of 55°C (130°F). Solar flux incident on the cask must be included.

Spent fuel assemblies give off the greatest amount of heat when they are first extracted from the reactor. After extraction, assemblies are stored for several months until they "cool down" to acceptable levels. Cask thermal restrictions, therefore, affect both assembly storage time and the number of assemblies that can be shipped in one cask.

This report presents the results of a detailed parametric evaluation of the thermal performance of some of these cask concepts during normal shipment. The

results are presented in a series of graphs which a designer can use to determine the effect of design and operational options. An overview of heat transfer associated with both normal shipping and loading conditions is found in Reference 3.

ANALYSIS

Section views of the cask are shown in Figures 1 and 2. The cask may be thought of as two distinct parts: the inner cavity which holds the fuel arrays and the external cask body which contains the radiation shielding and provides the structural strength. The inner basket modeled here consists of twelve steel pipes. Steel canisters, containing the fuel arrays, are placed inside the pipes. The space between the pipe and the canister is filled with helium. The fuel array may be packed in either helium or liquid sodium. The space between the pipes and the outer cask is either pressurized helium or aluminum.

The outer cask is composed of a layer of steel, a uranium gamma ray shield, a second layer of steel, a boron impregnated beechwood neutron shield, an outside layer of steel, and external steel fins. Embedded in the neutron shield are heat conducting fins made of steel or copper. The linear fin densities, both internal and external, are parameters as are all emissivities. All steels are 304 stainless. When aluminum is used in the inner basket, it is assumed that the aluminum is in intimate contact with the steel (zero contact resistance). The effect of non-zero contact resistance has been evaluated (see Reference 3).

In order to evaluate the individual influences of the large number of controlling parameters, the heat transfer from the fuel pins to the environment is divided into six parts:

(1) Radiation/convection from the outside surface of the cask to the environment.

(2) Conduction through the steel walls, neutron shield and gamma shield.

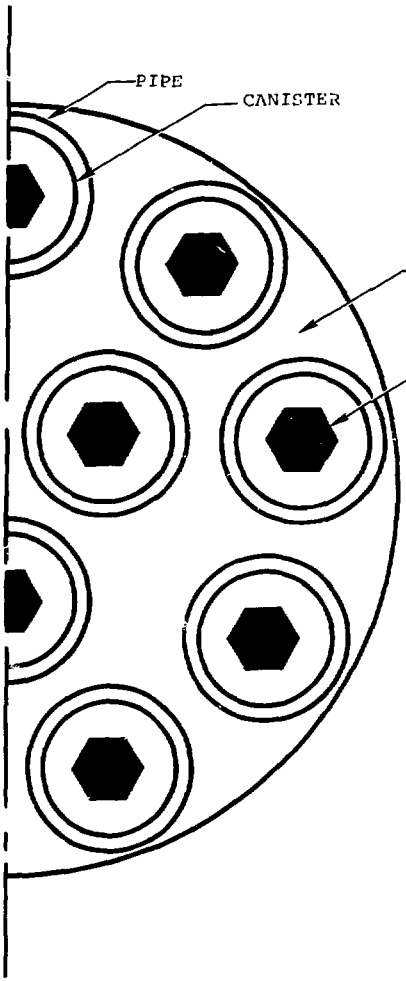

Hex Diameter (Flat to Flat)	0.1280 m
Canister I.D.	0.1651 m
O.D.	0.1778 m
Pipe I.D.	0.2064 m
O.D.	0.2190 m
Basket O.D.	0.7588 m
Center Radius (Inner Pipes)	0.1429 m
Center Radius (Outer Pipes)	0.3794 m

FIGURE 1. Inner Cask

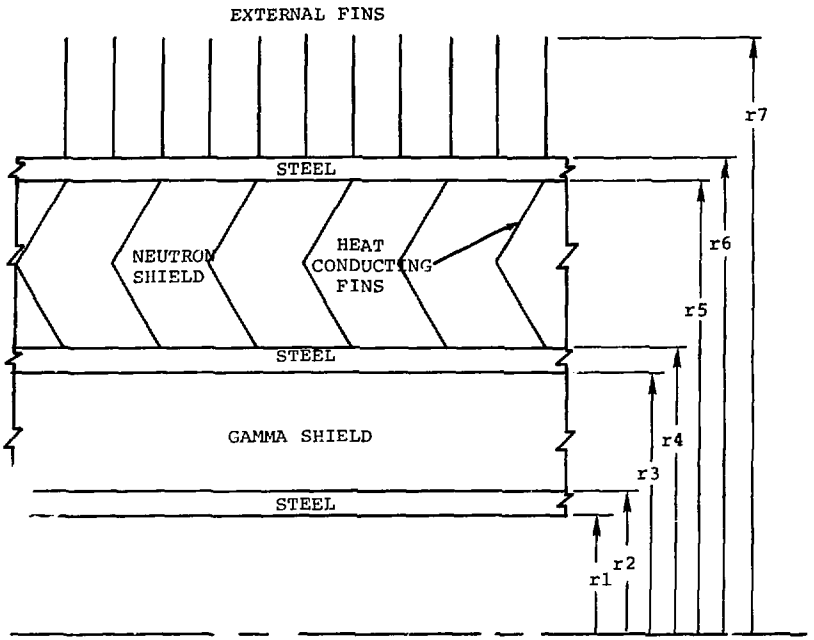

r1 = 0.4921 m

r2 = 0.5302 m

r3 = 0.5937 m

r4 = 0.5963 m

r5 = 0.9011 m

r6 = 0.9392 m

r7 = 1.0408 m

FIGURE 2. External Cask Cross Section

(3) Radiation/convection or conduction from the pipes to the steel inner containment wall of the outer cask.

(4) Convection/radiation from the canister to the pipe.

(5) Heat transfer by convection and radiation from the surface of the hexagonal fuel array to the canister.

(6) Relationship between maximum pin temperature and fuel array surface temperature.

The temperature drops across the separate sections of the cask are computed as functions of the cask thermal loading. The total temperature drop may be determined by summing the drops across the separate sections.

The calculations are one-dimensional and are based on a uniform axial power density. Thus, they are valid only for the center portion of the cask where the heat-generating sections of the pins are located.

The following assumptions have been used throughout the analysis:

(1) Circumferential variations in the temperature may be ignored. This assumption is valid only where similar heat sources are distributed somewhat uniformly about the inner perimeter of the cask. For cases where the cask is unevenly loaded, the temperature increases predicted must be considered as lower limits.

(2) Radiation may be superimposed upon both convection and conduction. In other words, gases are optically thin for the given dimensions.

(3) The effect of pressure upon convection may be included using a density correction factor in the Rayleigh number. More specifically, the helium density is assumed to obey the ideal gas law for constant temperatures. It is assumed that all other properties are independent of pressure.

(4) All contact resistances are ignored. Data from Reference 3 demonstrate that contact resistances provide significant thermal barriers. Contact resistances should be considered in all future design efforts.

(5) Due to the nature of the convection relationship used for pipes in a cavity, it is assumed that all fuel arrays produce the same power.

(6) For reasons to be stated later, the inner three pipes are assumed to be empty. The use of these pipes will be addressed in later publications.

Additional assumptions are listed in each section which are necessary to make the problem solvable. The validity of these assumptions must be evaluated with future experimental efforts.

Heat Transfer from Cask Surface to Environment

Assumptions

(1) Circumferential variations in the solar flux are ignored. This is a necessary result of the one-dimensional approach.

(2) Conventional fin efficiencies apply to natural convection. Since conventional fin efficiencies are computed using a constant heat transfer coefficient, and since heat transfer coefficients for natural convection are highly dependent on the surface configuration, the values generated for surface temperature rise must be viewed as approximations.

Governing Equations

(SOURCE POWER) + (INCIDENT SOLAR POWER) = (CONVECTED POWER) + (RADIATED POWER)

$$(NQ) + (Q_{SOL} A \alpha_{ve}) = [\bar{h} A_o (\frac{A}{A_o}) (T_{SURFACE} - T_{AMBIENT})] + [\sigma \varepsilon_e A_o (T^4_{SURFACE} - T^4_{AMBIENT})]$$

where,

$$\frac{A}{A_o} = 1 + 2n\eta_f L_{fin} \qquad \text{(Ref. 4)}$$

$$\eta_f = \frac{\tanh\sqrt{2\bar{h}L^2_{fin}/(k_{fin}t_{fin})}}{\sqrt{2\bar{h}L^2_{fin}/(k_{fin}t_{fin})}}$$

$$\bar{h} = 1.2424 \Delta T^{1/3} \text{ W/m}^2\text{-}^\circ\text{C} \qquad \text{(Ref. 5)}$$

$$\varepsilon_e = \left[1 + \frac{S}{S + 2L_{fin}} \left(\frac{1}{\varepsilon} - 1\right)\right]^{-1} \qquad \text{(Ref. 1)}$$

$$\alpha_{ve} = \left[1 + \frac{S}{S + 2L_{fin}} \left(\frac{1}{\alpha_v} - 1\right)\right]^{-1}$$

$$S = \frac{1 - nt}{n}$$

$$k_{fin} = 13.8 \text{ W/m}^\circ\text{C}$$

$$\left.\begin{matrix} \varepsilon = 0.3 \\ \alpha = 0.3 \end{matrix}\right\} \text{Untreated Surface}$$

$$\left.\begin{matrix} \varepsilon = 0.8 \\ \alpha_v = 0.2 \end{matrix}\right\} \text{Selective Surface}$$

$$L_{fin} = 0.1016 \text{ m}$$

$$Q_{SOL} = 290 \text{ W/m}^2$$

Solution

$$\Delta T = (NQ + Q_{SOL} A \alpha_{ve}) / \left[\bar{h} A_c \left(\frac{A}{A_o}\right) + \sigma \varepsilon_e A_o (T^2_{SURFACE} + T^2_{AMBIENT})(T_{SURFACE} + T_{AMBIENT})\right] .$$

The above equation is solved using an iterative technique. An initial temperature rise is selected. From this, a value for the surface temperature and the heat transfer coefficient is calculated. These values are then used in the above equation to compute a new temperature rise. The process is repeated until convergence is obtained.

Results are plotted in Figures 3 and 4. Comparing the graphs, one sees that while a selective surface lowers the cask surface temperature, the difference is not overwhelming. Before a costly selective surface is chosen, a parametric study of the effect of emissivity should be performed.

Conduction Through Outer Cask

Two materials are being considered for the neutron shield: borated beechwood and boron carbide in a copper matrix. Of the two, only the former has known thermal properties. Uranium is used as the gamma shield.

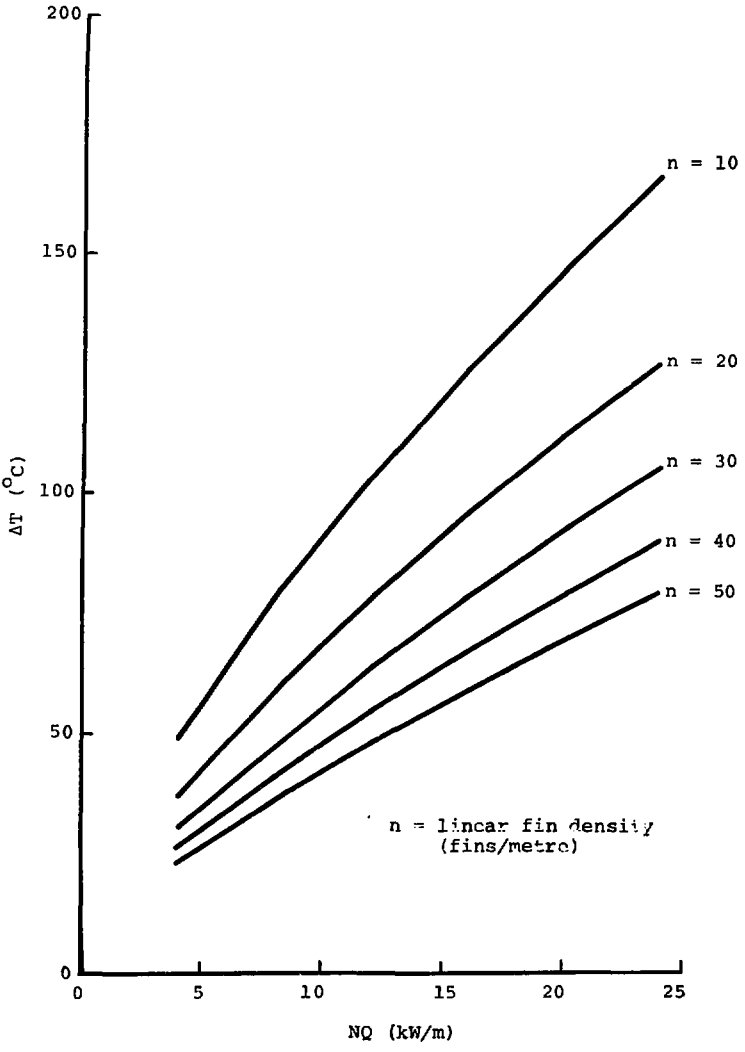

FIGURE 3. Temperature Rise at the Outer Surface of the Cask Versus Axial Power Density for $\varepsilon = \alpha = 0.3$

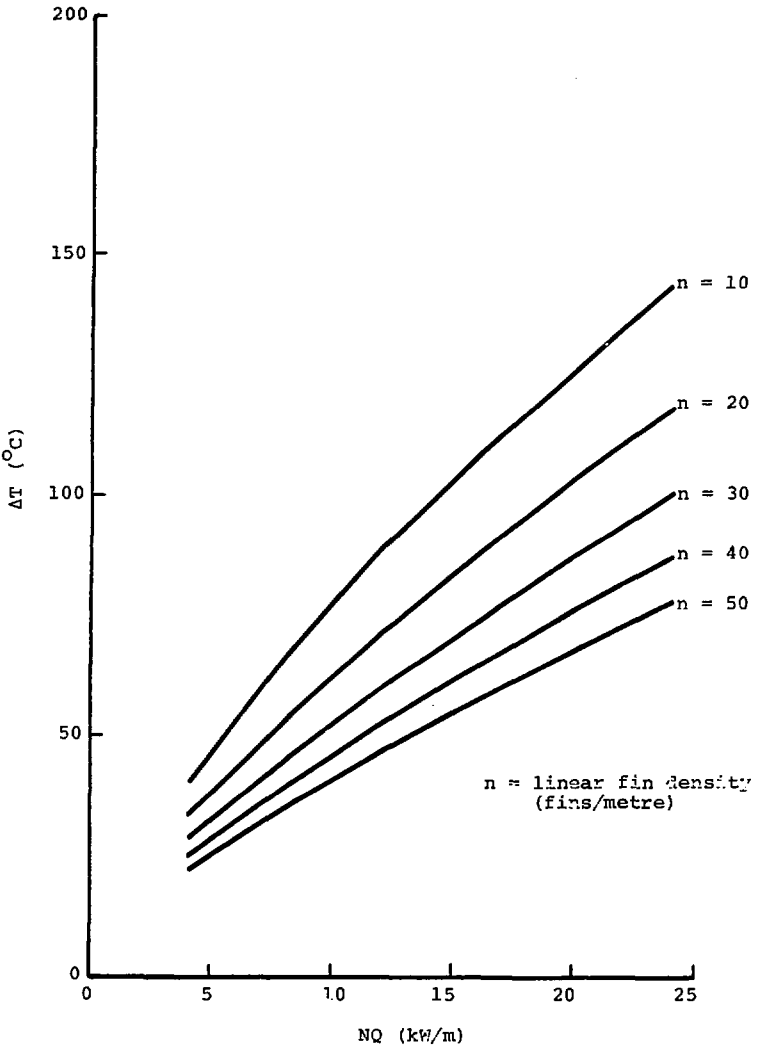

FIGURE 4. Temperature Rise at the Outer Surface of the Cask Versus Axial Power Density for $\varepsilon = 0.8$, $\alpha_v = 0.2$ (Selective Surface)

Equations

For conduction through a cylindrical shell:

$$\frac{\Delta K}{Q} = \frac{\ell n(r_o/r_i)}{2\pi k} \quad , \qquad \text{(Ref. 3)}$$

$k_{URANIUM}$ 23 W/m°C

$k_{BEECHWOOD}$ 0.2 W/m°C

k_{STEEL} 13.8 W/m°C

Layers

r (m)	Material
0.4921	STEEL #1
0.5302	URANIUM
0.5937	STEEL #2
0.5963	BEECHWOOD
0.9011	STEEL #3
0.9392	

Solution

Layer	ΔT/(NQ) (°C/kW/m)
STEEL #1	0.860
URANIUM	0.783
STEEL #2	0.050
BEECHWOOD	328.6
STEEL #3	0.978

Note that the controlling temperature drop occurs across the beechwood neutron shield - 328.6°C/kW/m of power.

Effect of Heat Transfer Fins in the Neutron Shield Layer

In order to decrease the temperature difference across the neutron shield, it has been proposed that internal fins be added to the neutron shield.[4] It is, therefore, of interest to estimate the effect of such fins.

Assumptions

(1) The fin length is two times the shield thickness; fins are angled through the shield to retain shielding property.

(2) Parallel thermal resistances model the composite adequately.

Solution

$$\frac{k_{EFFECTIVE}}{k_{SHIELD}} = 1 + n_f t\left(\frac{k_{fin}}{2k_{SHIELD}} - 1\right) \quad .$$

Results are shown in Figure 5. It is evident from the graph that copper fins are superior to steel fins (3 to 20 times the increase in effective conductivity) and should be used if possible. Note that with the fins, the temperature drop across the borated beechwood may easily be reduced by one to two orders of magnitude.

Heat Transfer from Pipes to Steel Inner Containment Wall

A. Radiation/Convection in Helium-Filled Basket

Assumptions

(1) Convection in the cavity may be described by boundary layers at the pipe and cavity surfaces. The bulk temperature of the gas does not vary with position and the boundary layers do not interfere with one another. Referring to Figure 1, one suspects that this assumption does not hold. For this reason, the temperature increases predicted should be viewed as lower bounds.

(2) Radiative heat transfer may be approximated using a two surface gray diffuse configuration factor. Because of this assumption, the interior three pipes have been ignored when radiation is included.

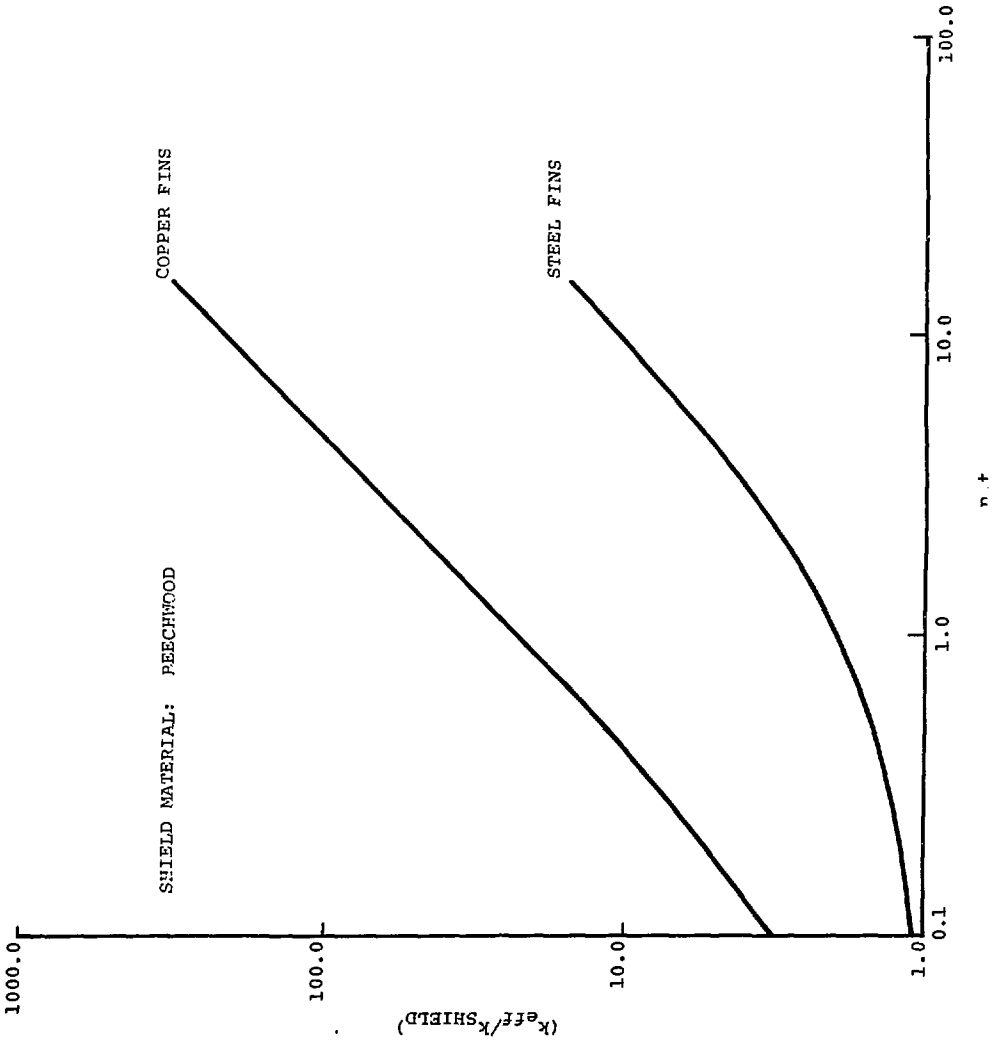

FIGURE 5. Effect of Heat Transfer Fins in Neutron Shield

Governing Equations

(SOURCE POWER) = (CONVECTED POWER) + (RADIATED POWER)

$$NQ = \overline{h'}(\pi D_{PIPE})(T_{PIPE} - T_{WALL}) + N\left(\frac{\pi D_{PIPE}}{2}\right)(\sigma\mathcal{F}_{P-W})(T_{PIPE}^4 - T_{WALL}^4) \quad ,$$

where,

$$\overline{h'} = \overline{Nu'_{P-W}}\, k_{GAS}/D_{PIPE} \quad . \qquad \text{(Ref. 7)}$$

$$\overline{Nu'_{P-W}} = \frac{2N}{\ell n(1 + 2/\overline{Nu}_{D_{PIPE}}) - N\ell n(1 - 2/\overline{Nu}_{D_{WALL}})} \quad ,$$

$$\overline{Nu}_{D_{PIPE}} = \left\{\left[0.518Ra_{D_{PIPE}}^{1/4}\left\langle 1 + \left(\frac{0.559}{Pr}\right)^{3/5}\right\rangle^{-5/12}\right]^{15} + \left[0.1Ra_{D_{PIPE}}^{1/3}\right]^{15}\right\}^{1/15} \quad ,$$

$$\overline{Nu}_{D_{WALL}} = \left\{\left[\left\langle\left(\frac{2}{1 - e^{-0.25}}\right)^{5/3} + \left(0.587GRa_{D_{WALL}}^{1/4}\right)^{5/3}\right\rangle^{3/5}\right]^{15} + \left[0.1Ra_{D_{WALL}}^{1/3}\right]^{15}\right\}^{1/15} \quad ,$$

$$G = \left[\left(1 + \frac{0.6}{Pr^{0.7}}\right)^{-5} + (0.4 + 2.6Pr^{0.7})^{-5}\right]^{-1/5}$$

$$\frac{T_{GAS} - T_{WALL}}{T_{PIPE} - T_{GAS}} = \frac{-N\ell n(1 - 2/\overline{Nu}_{D_{WALL}})}{\ell n(1 + 2/\overline{Nu}_{D_{PIPE}})} \quad ,$$

$$Ra = Pr\left(\frac{g\beta}{\nu^2}\right)\rho^2 D^3 \Delta T \quad ,$$

where $\frac{g\beta}{\nu^2}$ is evaluated at one atmosphere and pressure, P, is in atmospheres.

$$\mathcal{F} \approx 0.8\left[\frac{1}{\epsilon_{PIPE}} + \left(\frac{D_{PIPE}/2}{D_{WALL}/2}\right)\left(\frac{1}{\epsilon_{WALL}} - 1\right)\right]^{-1} ,$$

$$\epsilon_{PIPE} = \epsilon_{WALL}$$

ϵ	$\mathcal{F}$
0.0	0.000
0.1	0.040
0.3	0.140
0.9	0.654

D_{PIPE} = 0.2190m

D_{WALL} = 0.9842m

P = 1, 5, 10, 20 atm

Solution

$$T_{PIPE} - T_{WALL} = \frac{NQ}{\left[\pi\overline{Nu}'_{P-W}k + \frac{N\pi D_{PIPE}}{2}\sigma\mathcal{F}_{P-W}(T^2_{PIPE} + T^2_{WALL})(T_{PIPE} + T_{WALL})\right]} .$$

This equation was solved in a manner similar to that used in Section I. Results are shown in Figures 6 through 17. The strong effect of emissivity on the temperature rise is evident on each graph. Comparing graphs for equal wall temperatures, one also finds a strong dependence on helium pressure. Thus, both are important design parameters.

B. Conduction Through an Aluminum Basket

Assumptions

(1) The energy flux is evenly distributed about the circumference of the pipe.

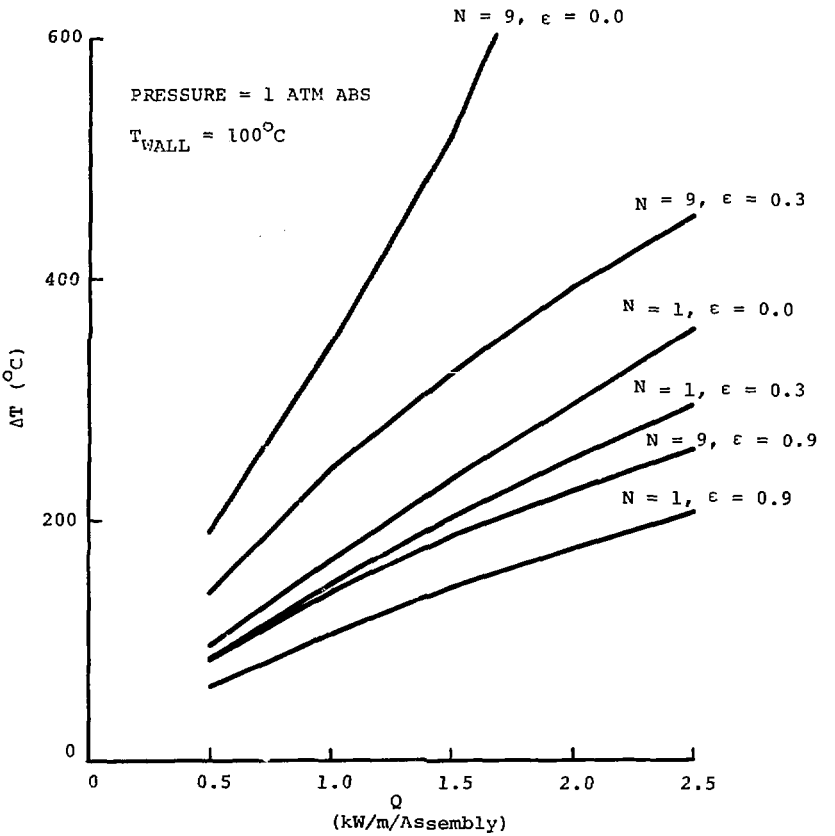

FIGURE 6. Temperature Rise Across a Helium-Filled Basket Versus Axial Power Density

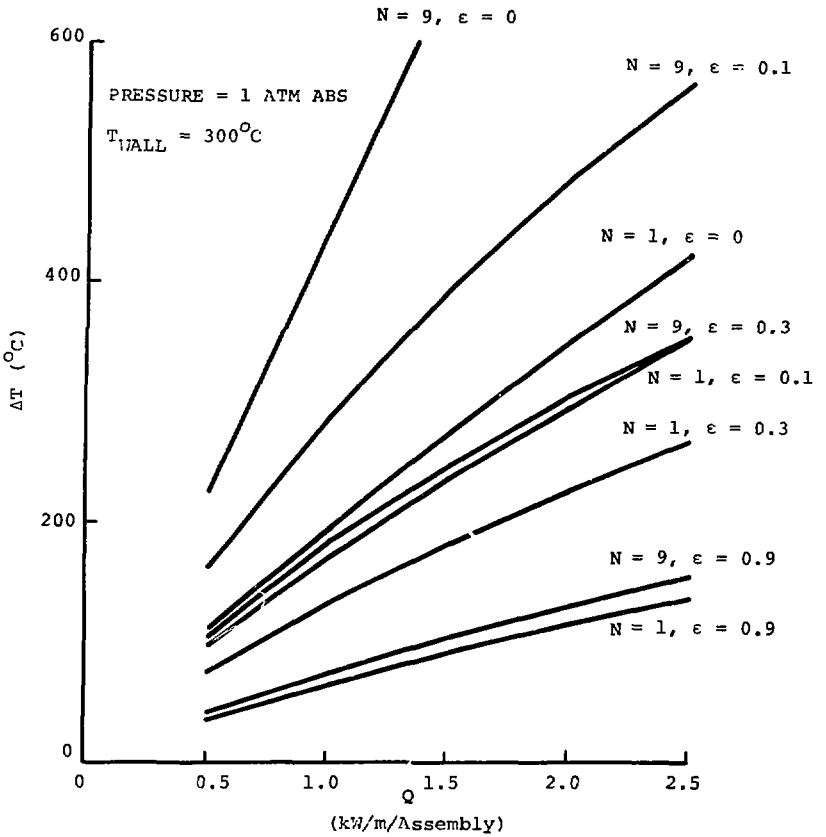

FIGURE 7. Temperature Rise Across a Helium-Filled Basket Versus Axial Power Density

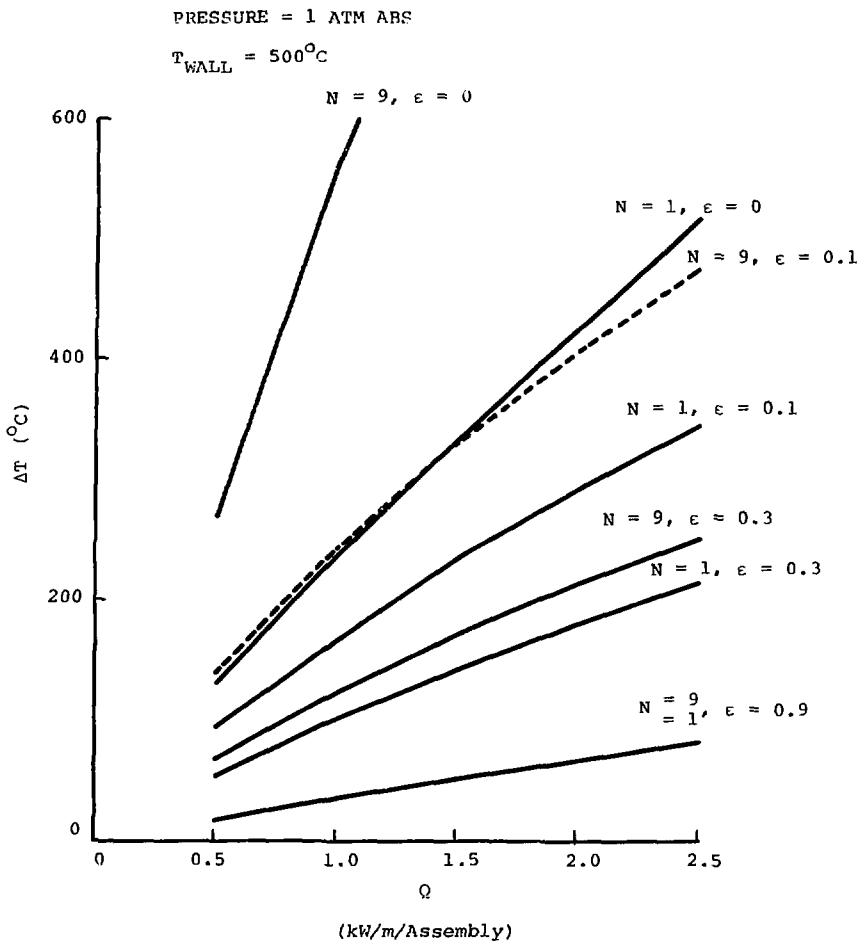

FIGURE 8. Temperature Rise Across a Helium-Filled Basket Versus Axial Power Density

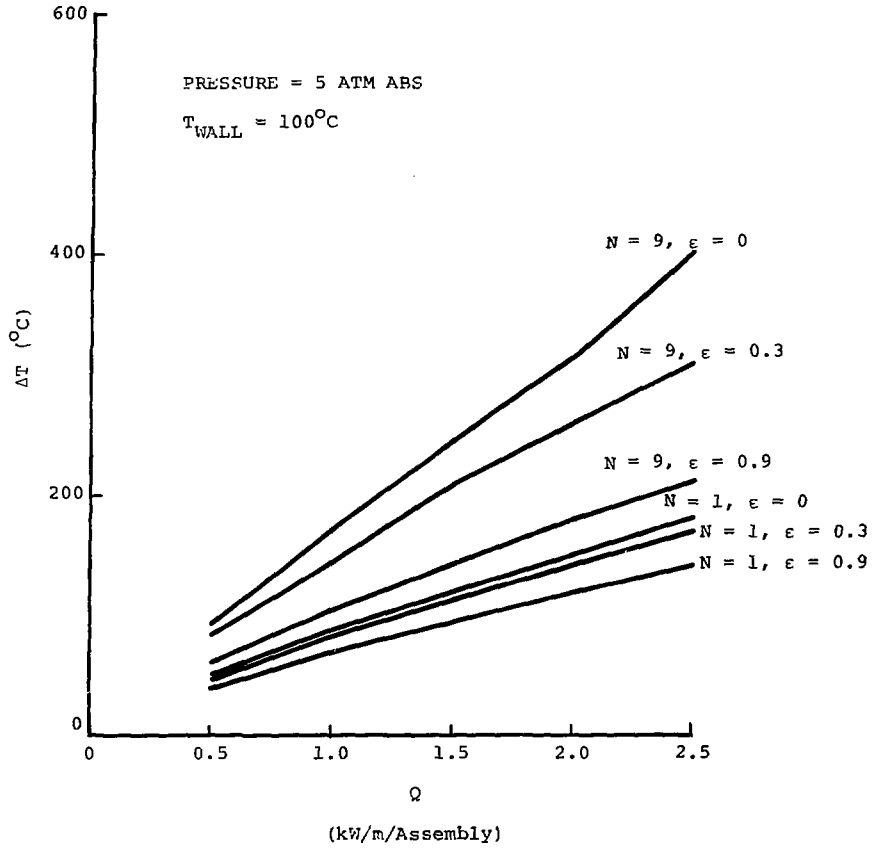

FIGURE 9. Temperature Rise Across a Helium-Filled Basket Versus Axial Power Density

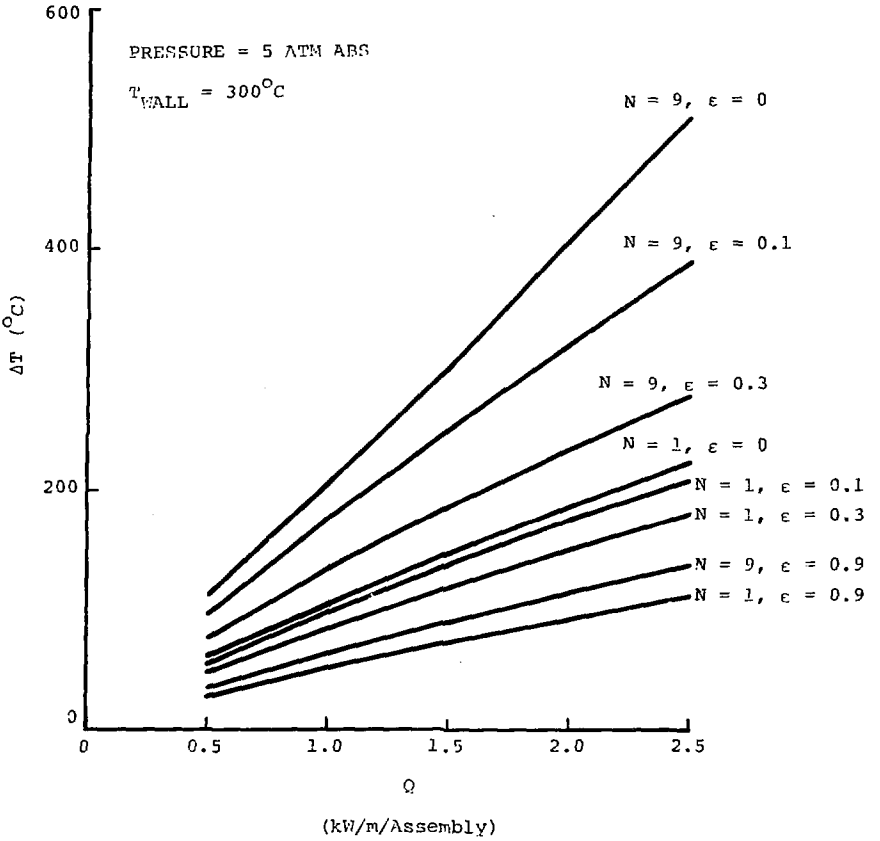

FIGURE 10. Temperature Rise Across a Helium-Filled Basket Versus Axial Power Density

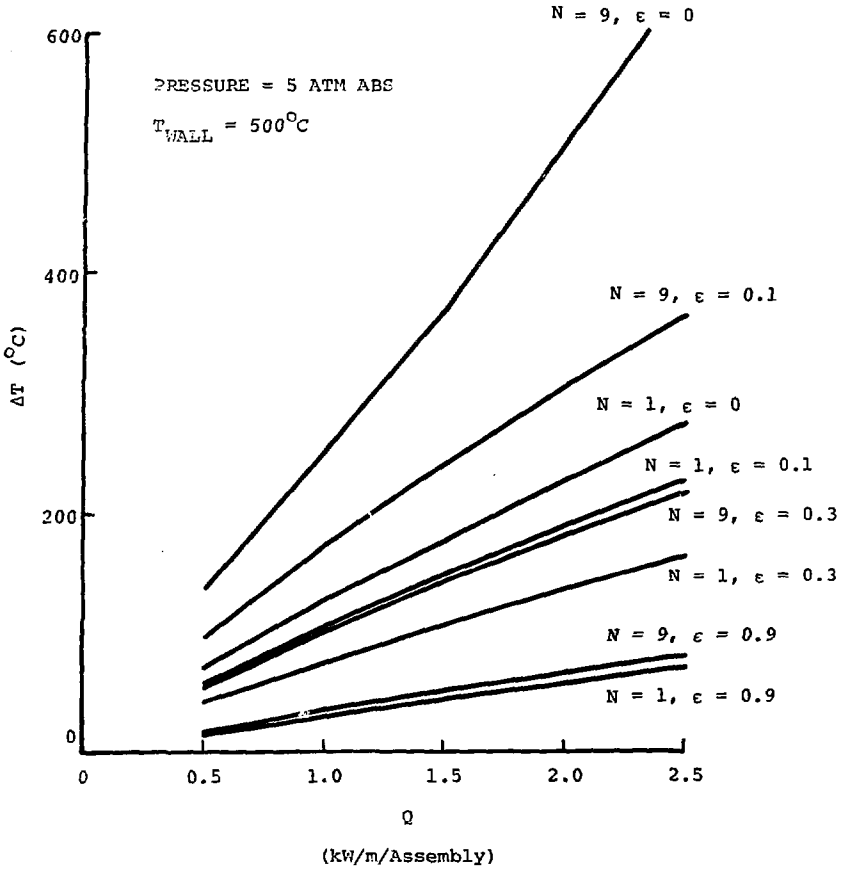

FIGURE 11. Temperature Rise Across a Helium-Filled Basket Versus Axial Power Density

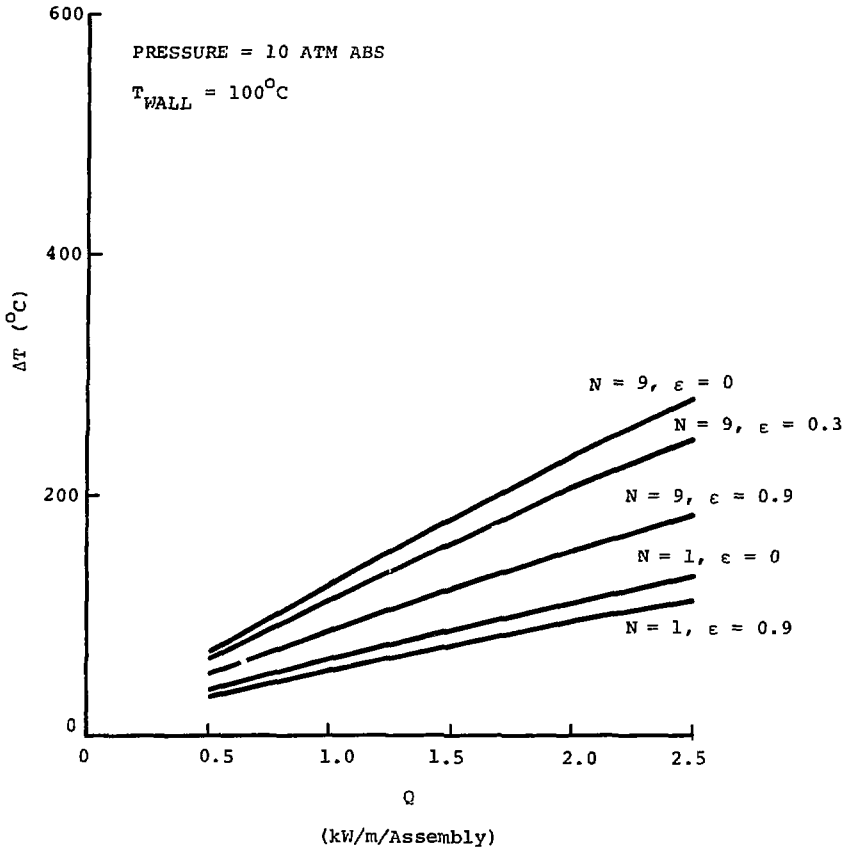

FIGURE 12. Temperature Rise Across a Helium-Filled Basket Versus Axial Power Density

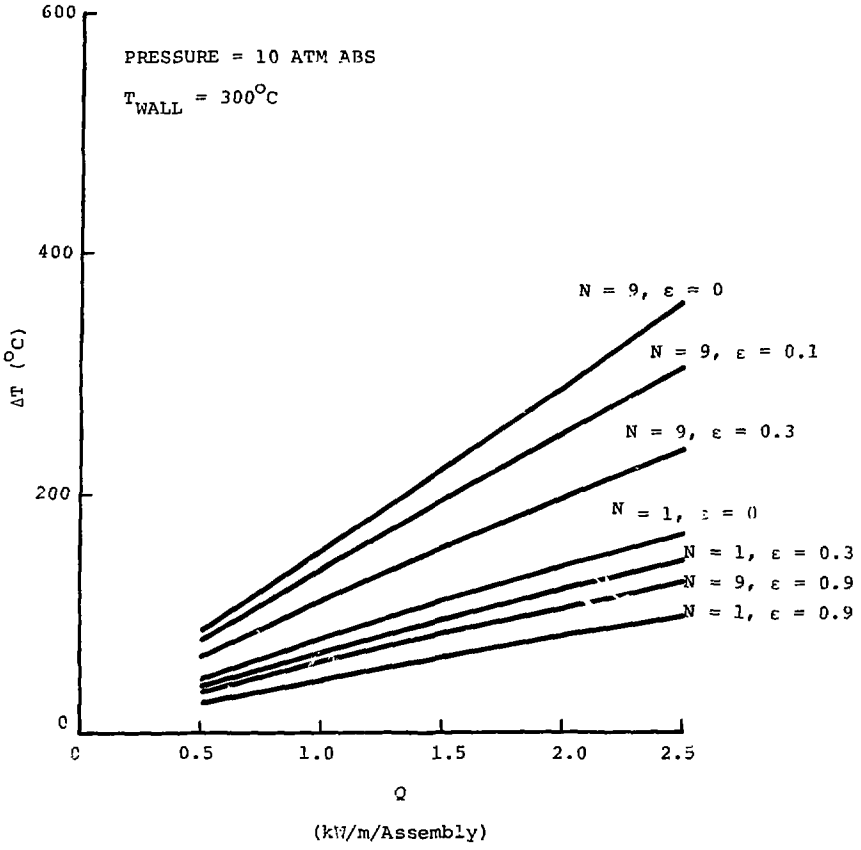

FIGURE 13. Temperature Rise Across a Helium-Filled Basket Versus Axial Power Density

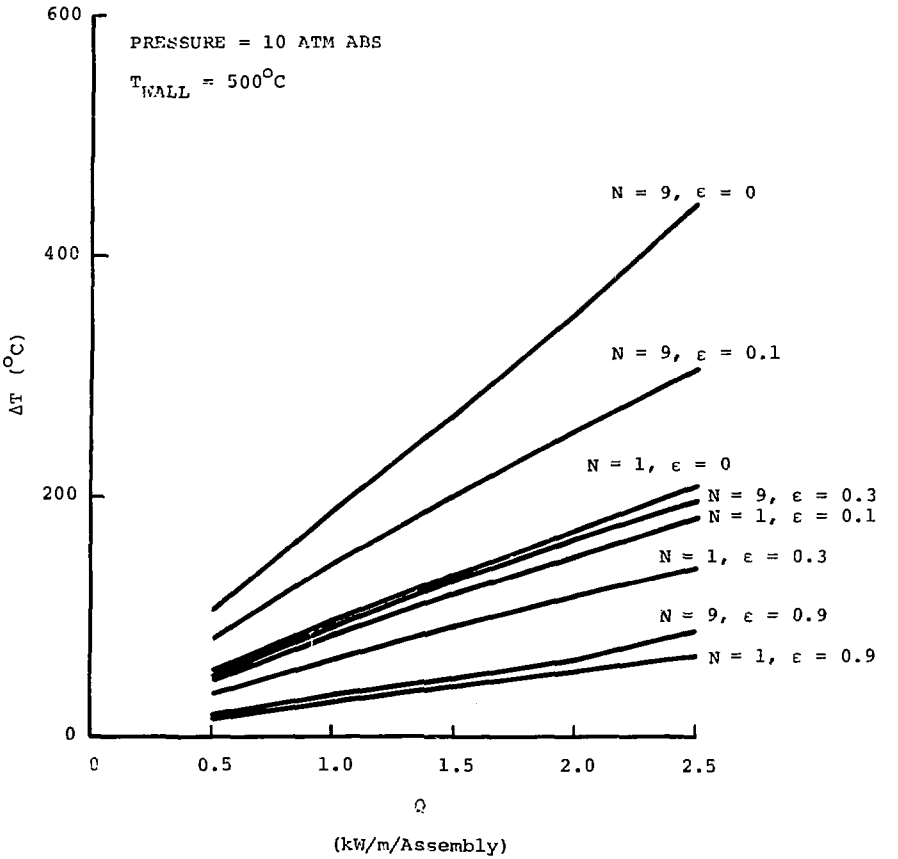

FIGURE 14. Temperature Rise Across a Helium-Filled Basket Versus Axial Power Density

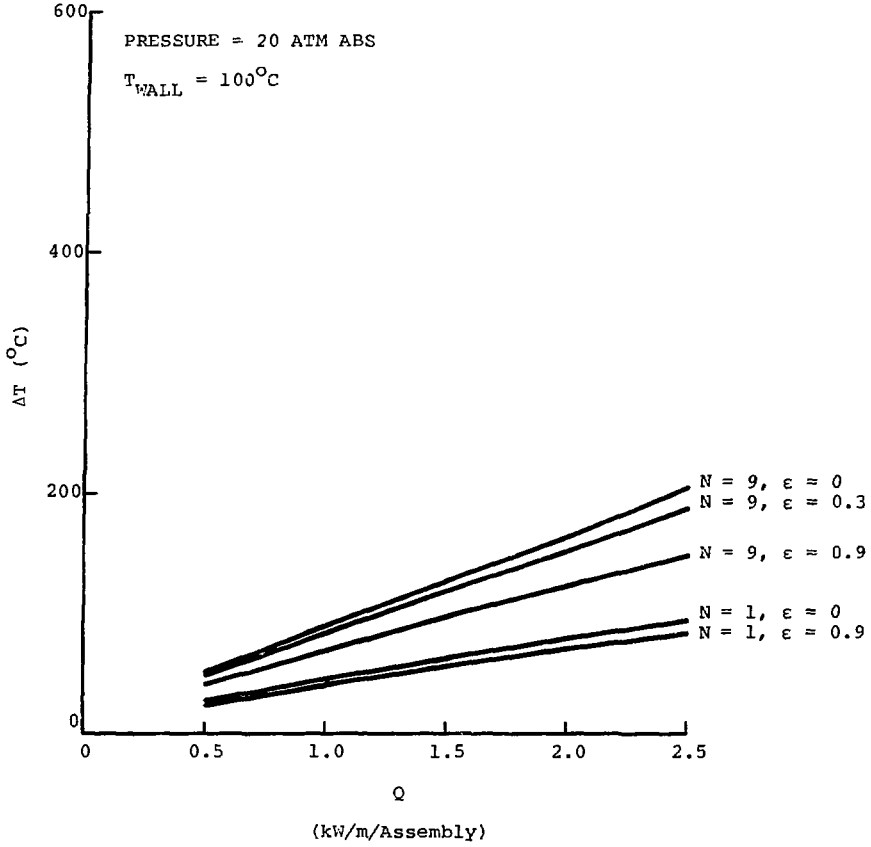

FIGURE 15. Temperature Rise Across a Helium-Filled Basket Versus Axial Power Density

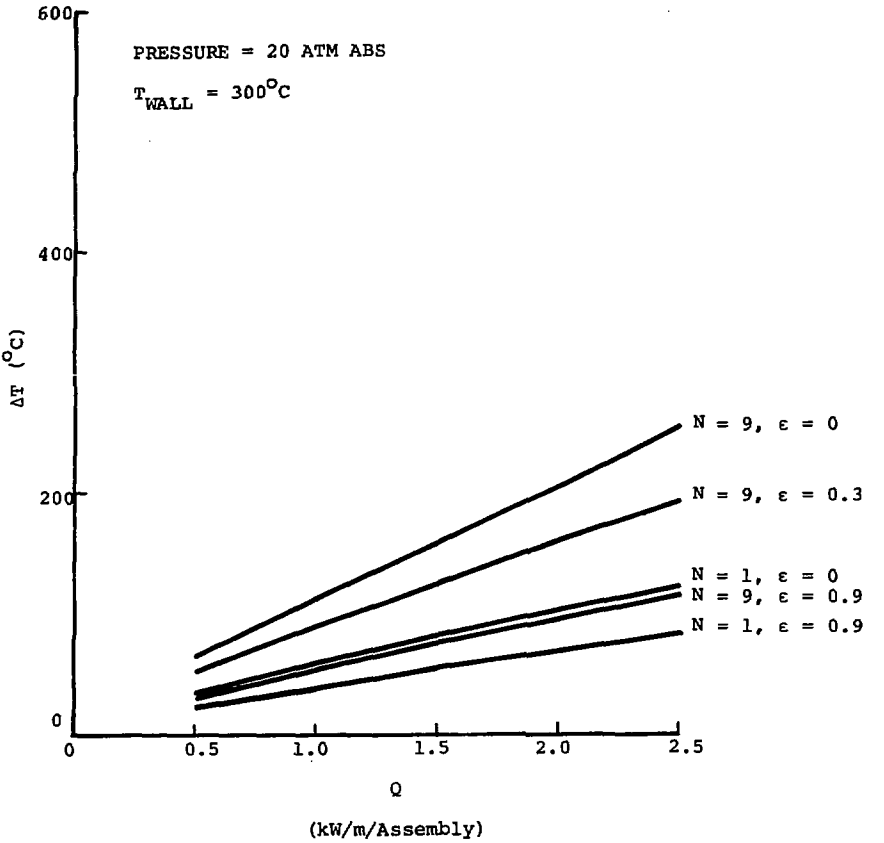

FIGURE 16. Temperature Rise Across a Helium-Filled Basket Versus Axial Power Density

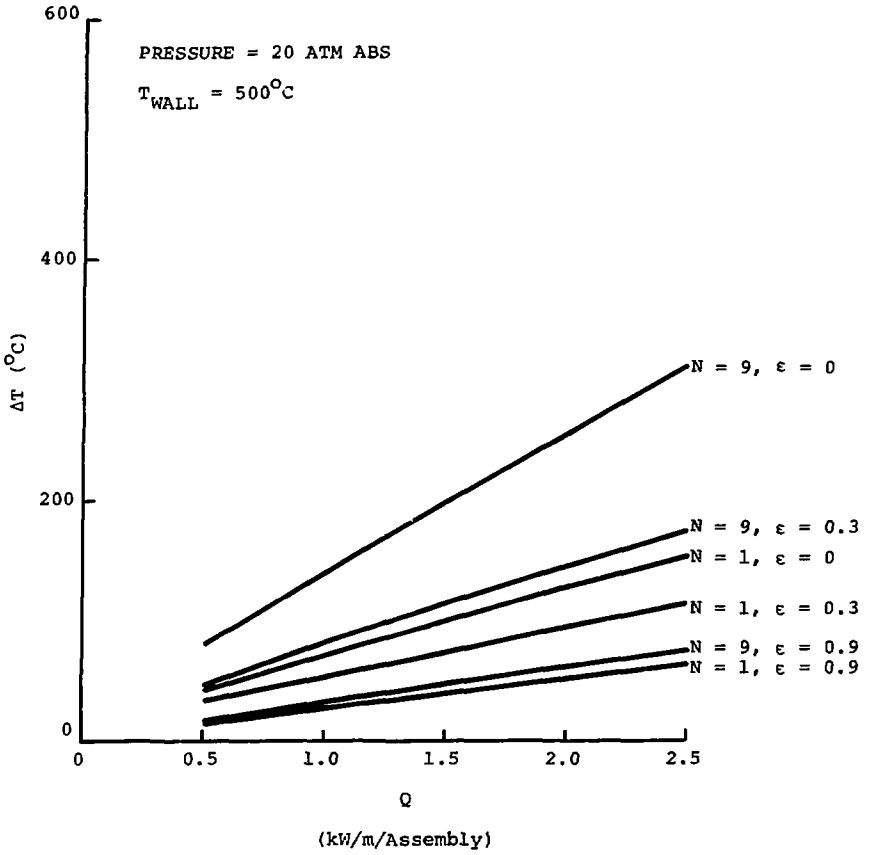

FIGURE 17. Temperature Rise Across a Helium-Filled Basket Versus Axial Power Density

Equation

Conduction Equation

Solution

This problem was solved using the heat conduction code CINDA[8] for the assembly energy levels shown. The outer nine pipes were occupied in all runs. Figure 18 indicates a sensitivity of about 8°C/kW/m for this arrangement. Configurations where an inner pipe is also filled will produce higher temperatures than those shown.

Circumferential Temperature Variation in Pipe

One of the assumptions used in the computation of temperature rise between the pipes and the gamma shield for heat transfer via convection and radiation was that the circumferential temperature variation in the pipe could be ignored. Since radiative heat transfer between the pipe and the inner containment wall occurs on only one side of the pipe, it appeared worthwhile to investigate the conditions under which the assumption holds. Therefore, a model was constructed to estimate this variation.

Assumptions

(1) The heat source is uniformly distributed throughout the pipe. A linear power density of 2.5 kW/m is used.

(2) The shield temperature is 225°C.

(3) View factors are computed as in Part II.

(4) Only radiation is considered due to the uncertainty in the convective relationships.

Solution

Graphs of circumferential temperature variation as a function of angular position are shown in Figures 19 and 20. If a temperature variation of 30°C is considered acceptable, then copper or aluminum pipes having wall thicknesses of 0.01 m and 0.02 m, respectively, are recommended.

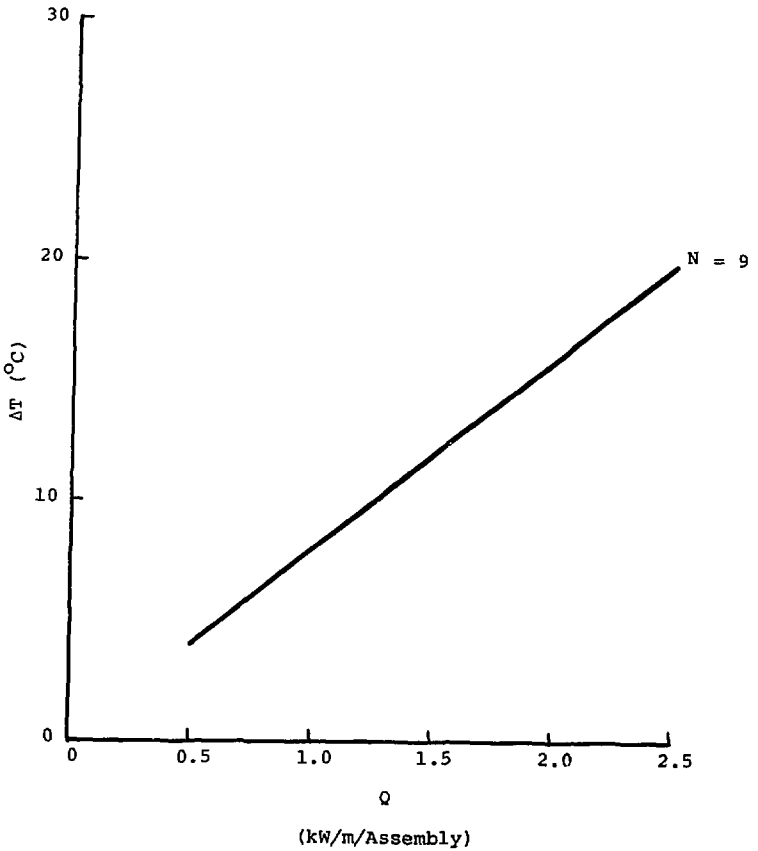

FIGURE 18. Temperature Rise Across an Aluminum Basket Versus Axial Power Density

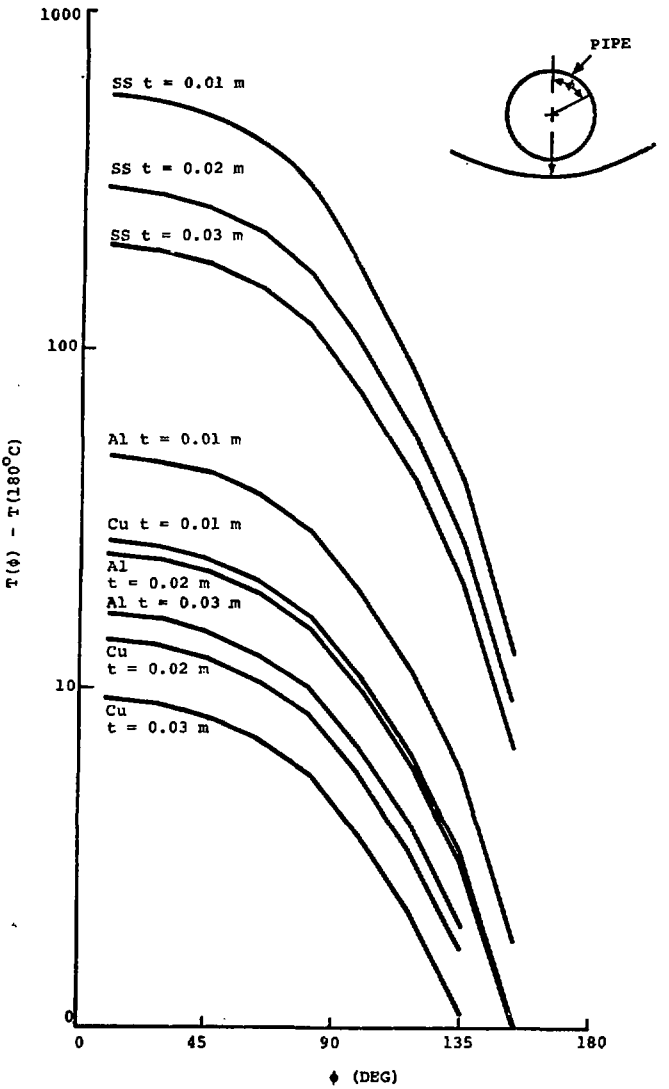

FIGURE 19. Temperature Difference Versus Circumferential Position for Pipe ($\varepsilon = 0.3$)

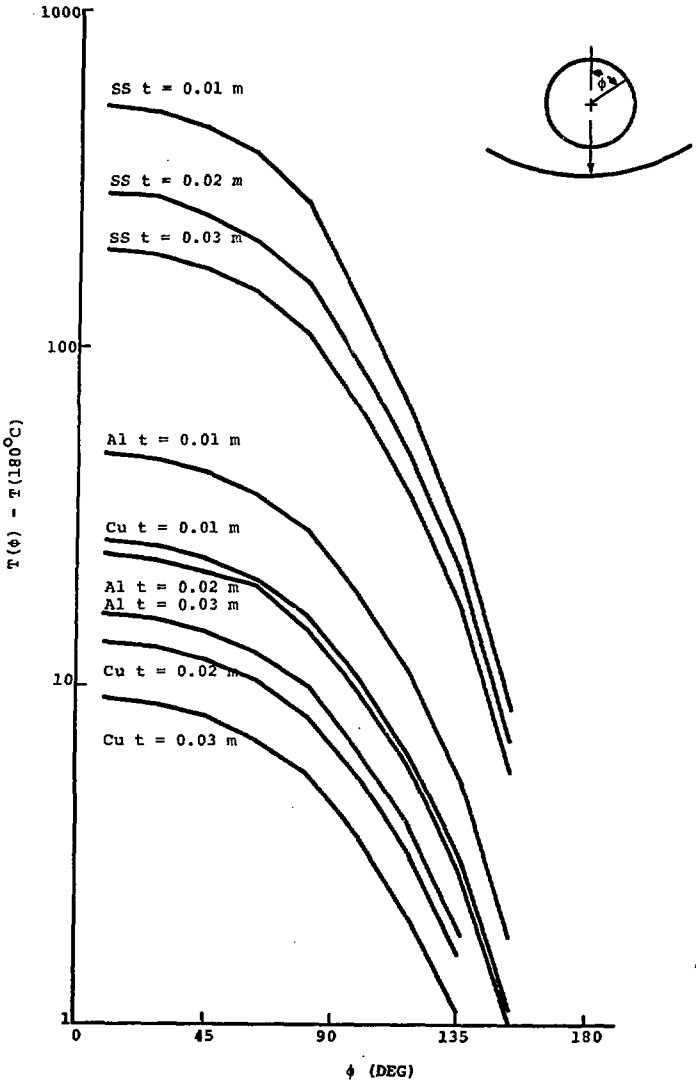

FIGURE 20. Temperature Difference Versus Circumferential Position for Pipe (ε = 0.9)

Heat Transfer from Canister to Pipe

Governing Equations

(SOURCE POWER) = (CONDUCTED OR CONVECTED POWER)
+ (RADIATED POWER)

$$Q = \frac{2\pi k Nu_\delta}{\ell n(D_{PIPE}/D_{CAN})} (T_{CAN} - T_{PIPE}) + \pi D_{CAN} \sigma \mathcal{F}_{C-P} (T_{CAN}^4 - T_{PIPE}^4) ,$$

$$Nu_\delta = 0.2\ Ra^{\frac{1}{4}} , \qquad \text{(Ref. 5)}$$

$$Ra = PrGr , \quad Pr = 0.7 ,$$

$$Gr = \left(\frac{g\beta}{\nu^2}\right) \rho^2 \left(\frac{D_{PIPE} - D_{CAN}}{2}\right)^3 (T_{CAN} - T_{PIPE}) ,$$

$$\mathcal{F}_{C-P} = \left[\frac{1}{\epsilon_{CAN}} + \frac{D_{CAN}}{D_{PIPE}} \left(\frac{1}{\epsilon_{CAN}} - 1\right)\right]^{-1} .$$

Solution

$$T_{CAN} - T_{PIPE} = Q/\left[Nu_\delta \frac{2\pi k}{\ell n(r_{PIPE}/r_{CAN})} + \pi D_{CAN} \sigma \mathcal{F}_{C-P} (T_{PIPE}^2 + T_{CAN}^2)(T_{PIPE} + T_{CAN})\right] .$$

This equation was solved in a manner similar to that used in Section I. Figures 21 through 23 confirm the strong dependence on surface emissivity seen in Figures 6 through 17. The influence of pressure is a strong function of wall temperature at lower helium pressures.

Heat Transfer from Hexagonal Fuel Array to Canister

A. Helium Filled Canister

Governing Equations

(SOURCE POWER) = (AREA)(HEAT TRANSFER COEFFICIENT)
(TEMPERATURE DIFFERENCE)

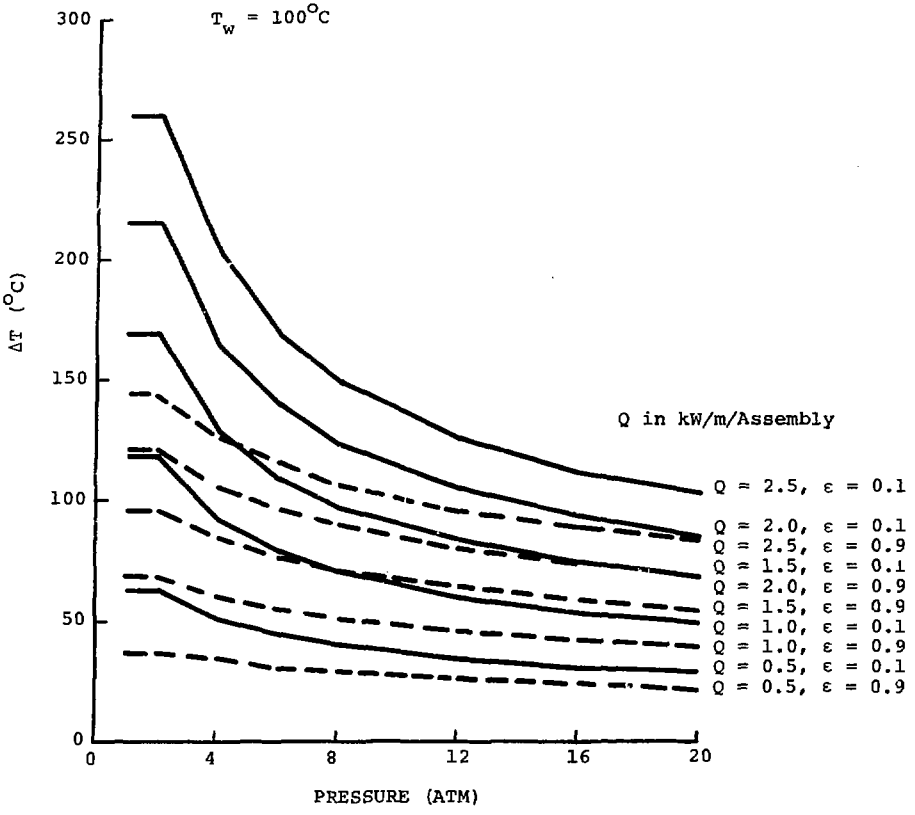

FIGURE 21. Temperature Rise Between Canister and Pipe Versus Helium Pressure

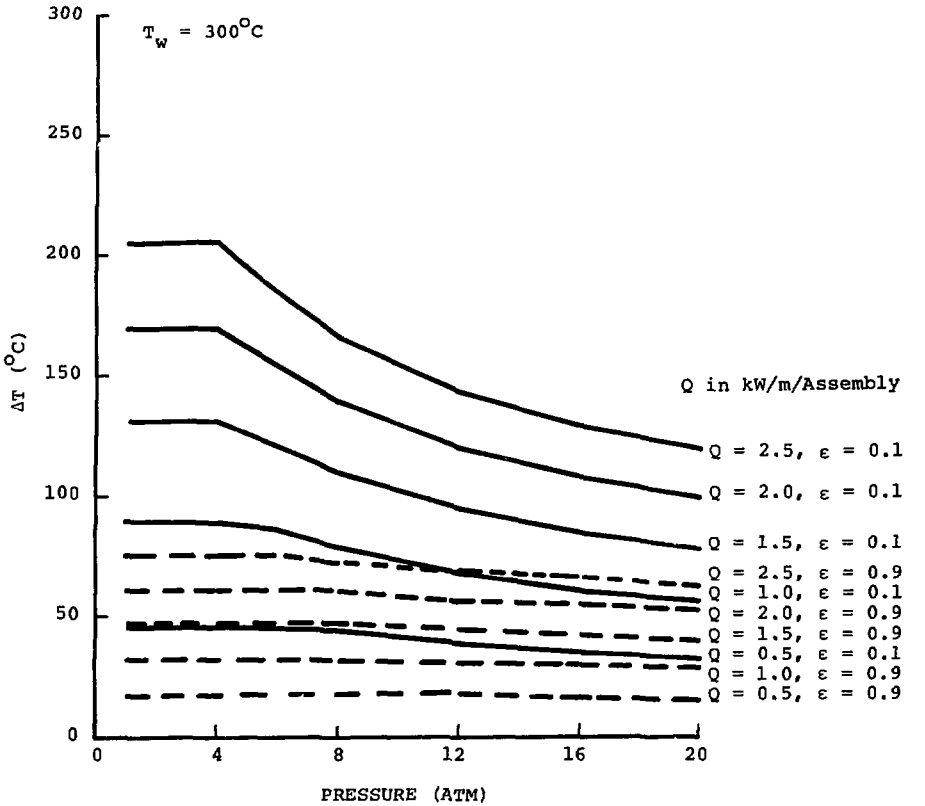

FIGURE 22. Temperature Rise Between Canister and Pipe Versus Helium Pressure

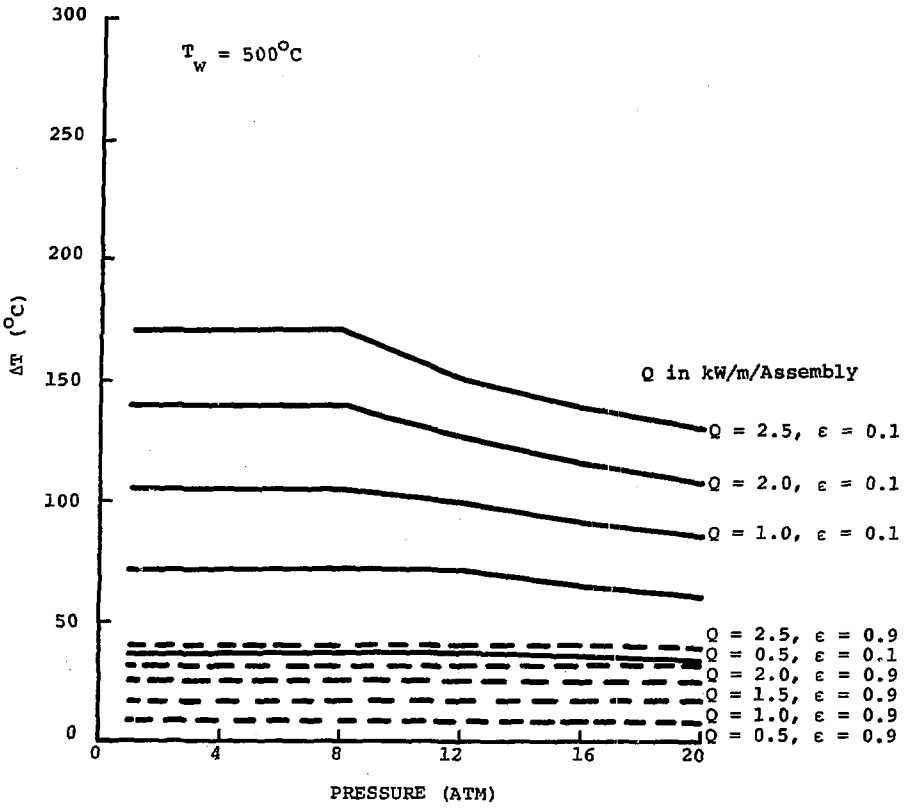

FIGURE 23. Temperature Rise Between Canister and Pipe Versus Helium Pressure

$$Q = (\pi D_{CAN})(h_{CAN})(T_{HEX} - T_{CAN}) \quad ,$$

$$Nu = 0.43\ Gr^{0.25} \quad , \qquad \text{(Ref. 3)}$$

$$Gr_m = \frac{g\beta}{\nu^2} P^2 \left[\sqrt{r_{HEX} r_{CAN}}\ \ell n \frac{r_{CAN}}{r_{HEX}}\right]^3 \Delta T \quad ,$$

$$Nu = h_{CAN}\left[r_{CAN}\ell n (r_{CAN}/r_{HEX})\right]/k \quad .$$

Solution

$$\Delta T = \frac{Q\ell n (r_{CAN}/r_{HEX})}{2\pi k Nu} \quad .$$

This equation was solved in a manner similar to that used in Section I. Figures 24 through 26 show a strong pressure influence on the array-canister temperature difference.

B. Sodium Filled Canister

Assumptions

For lack of a good correlation, assume the heat transfer takes place via conduction (see Section VII).

Governing Equations

$$Q \approx \frac{2\pi k}{\ell n (r_{CAN}/r_{HEX})} (T_{HEX} - T_{CAN}) \quad ,$$

$$r_{CAN} = 0.08255 \text{ m} \quad ,$$

$$r_{HEX} = 0.06401 \text{ m} \quad .$$

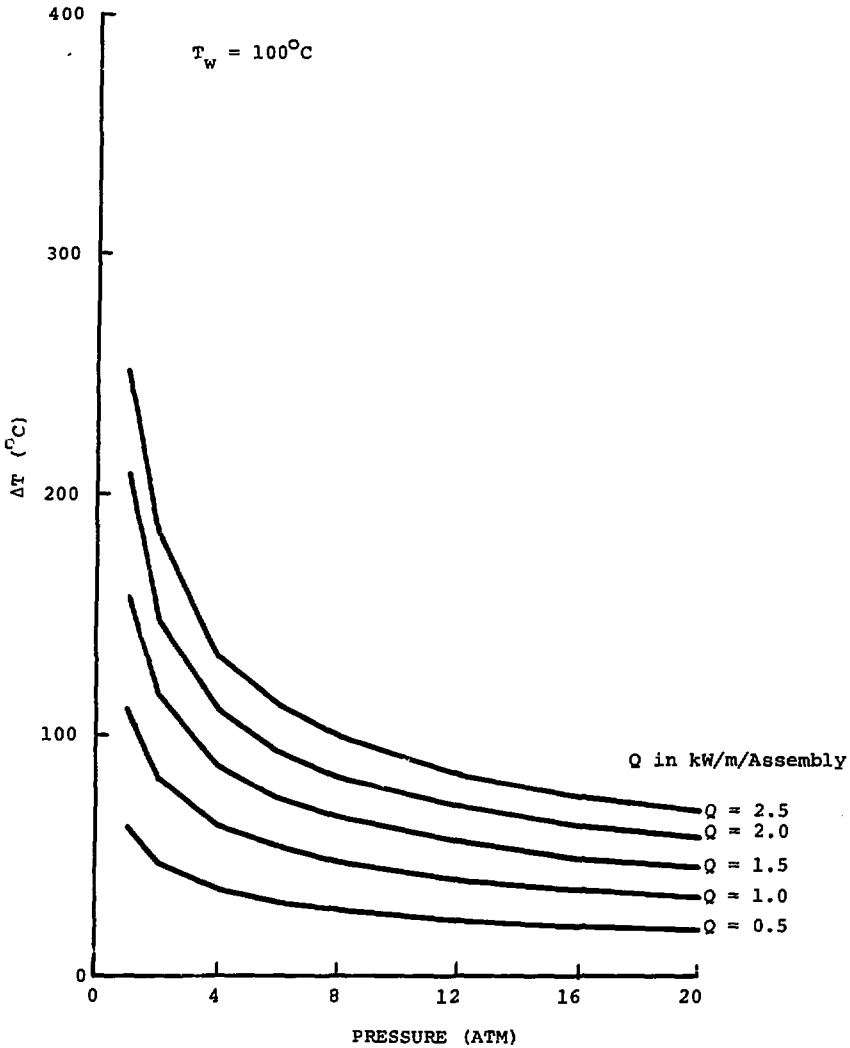

FIGURE 24. Temperature Rise Between Hexagonal Fuel Array and Canister Versus Helium Pressure

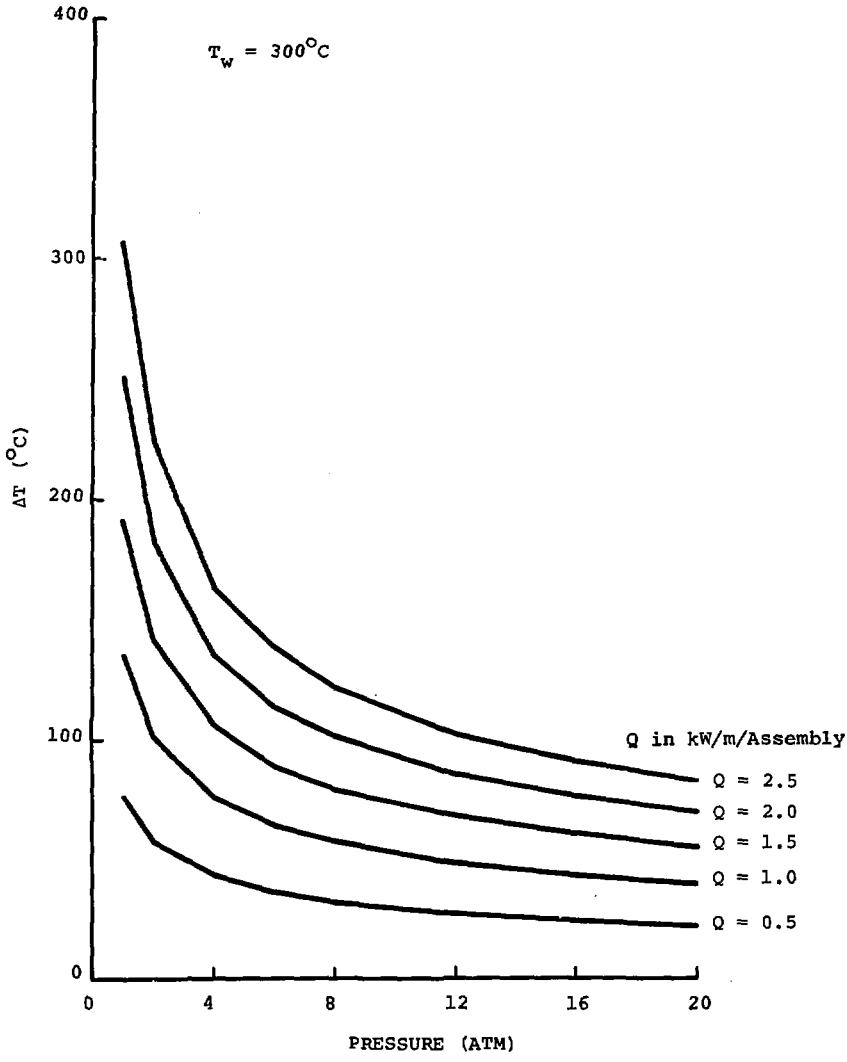

FIGURE 25. Temperature Rise Between Hexagonal Fuel Array and Canister Versus Helium Pressure

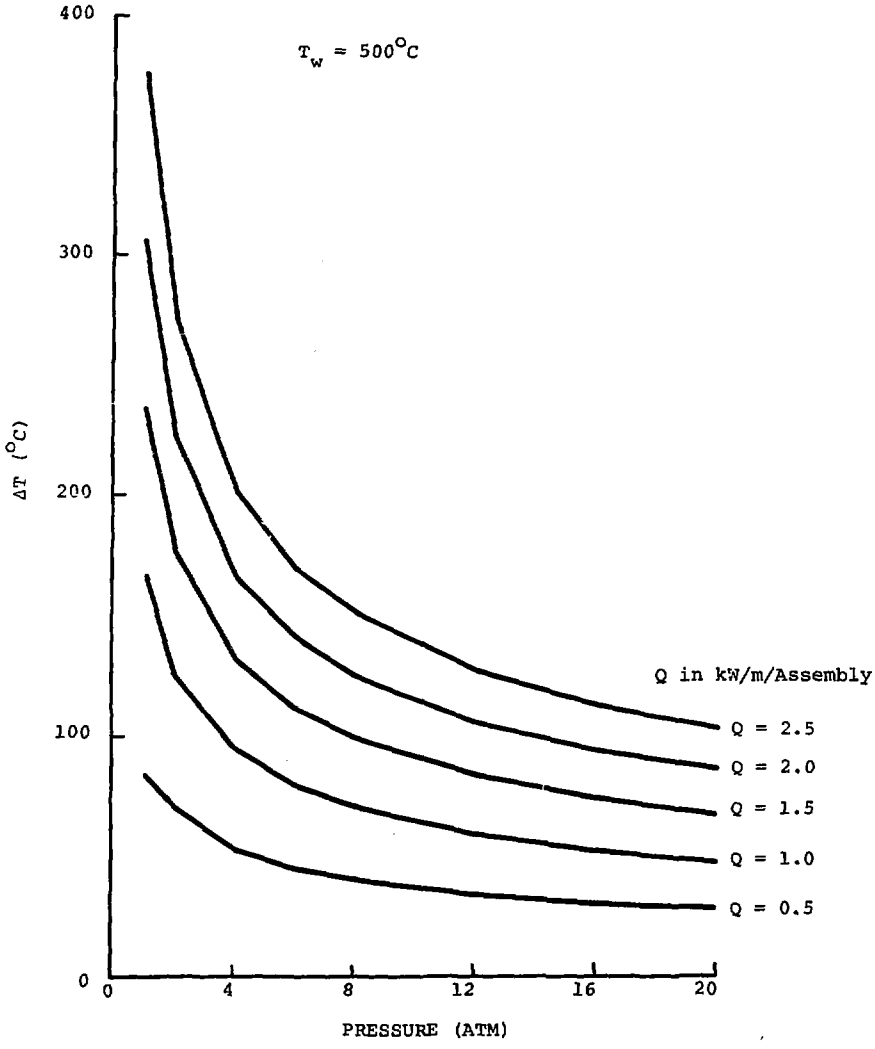

FIGURE 26. Temperature Rise Between Hexagonal Fuel Array and Canister Versus Helium Pressure

Solution

$$\frac{\Delta T}{Q} = 0.688^{\circ}C/\frac{kW}{m} \quad .$$

Sodium Correlations

To date, two sets of experiments have been conducted to determine the temperature increases that occur when a spent fuel array is packaged in a cylinder filled with sodium. The experiments were conducted at Oak Ridge National Laboratory[9] and the Nuclear Energy Research Center, Karlsrube, Germany.[10] The information generated from these experiments demonstrates the effectiveness of sodium as a coolant, however, attempts to correlate the data in terms of dimensionless parameters, such as those developed in Reference 3 for helium, have failed. This failure can be attributed to a number of things. First, temperature drops across the steel sections often overshadowed the temperature drop across the sodium. Second, the use of sodium adds a strong second dimension to the heat transfer, making it difficult to formulate a reasonable one-dimensional correlation. Two of the correlation attempts are seen in Figures 27 and 28. Since neither graph indicates a strongly recognizable relationship, conservative Nusselt number values of 1.0 and 0.3 are recommended for the hex-cylinder and pin-hex regions, respectively. Third, the German and Oak Ridge experiments involved fuel assemblies and pipes that differed both in orientation and geometry.

Computation of Hexagonal Array Wrapper Temperature

It is now of interest to identify several of the possible cask configurations and compute the hexagonal array wrapper temperatures that will occur in each case. Calculation of the pin temperature is deferred to a future section for reasons which will become evident later. The configurations considered are:

Option 1

1. Helium-filled basket
2. Helium-filled canister

Option 2

1. Aluminum basket
2. Helium-filled canister

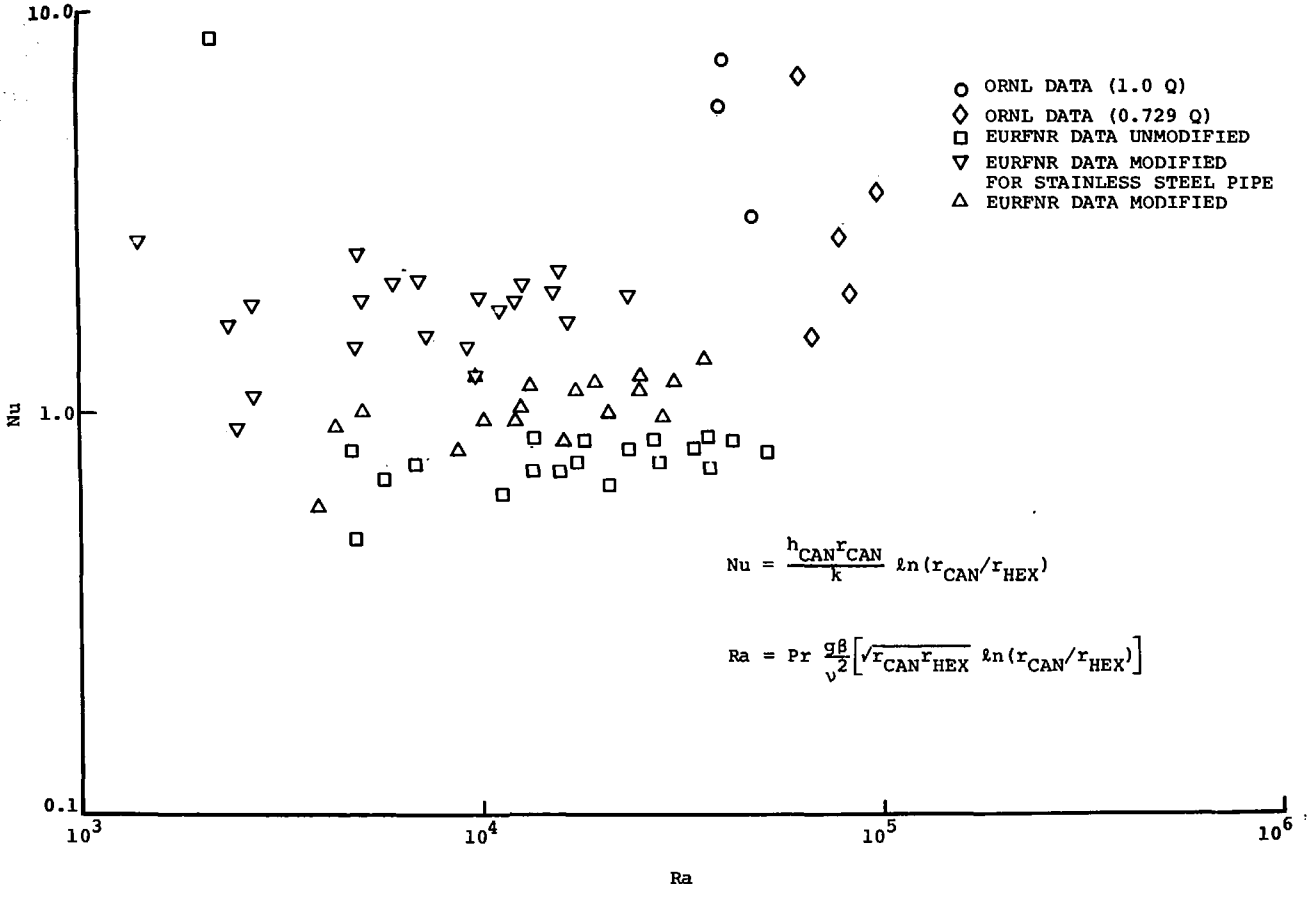

FIGURE 27. Nussult Number Versus Rayleigh Number for Hex-Cylinder Region of Fuel Array

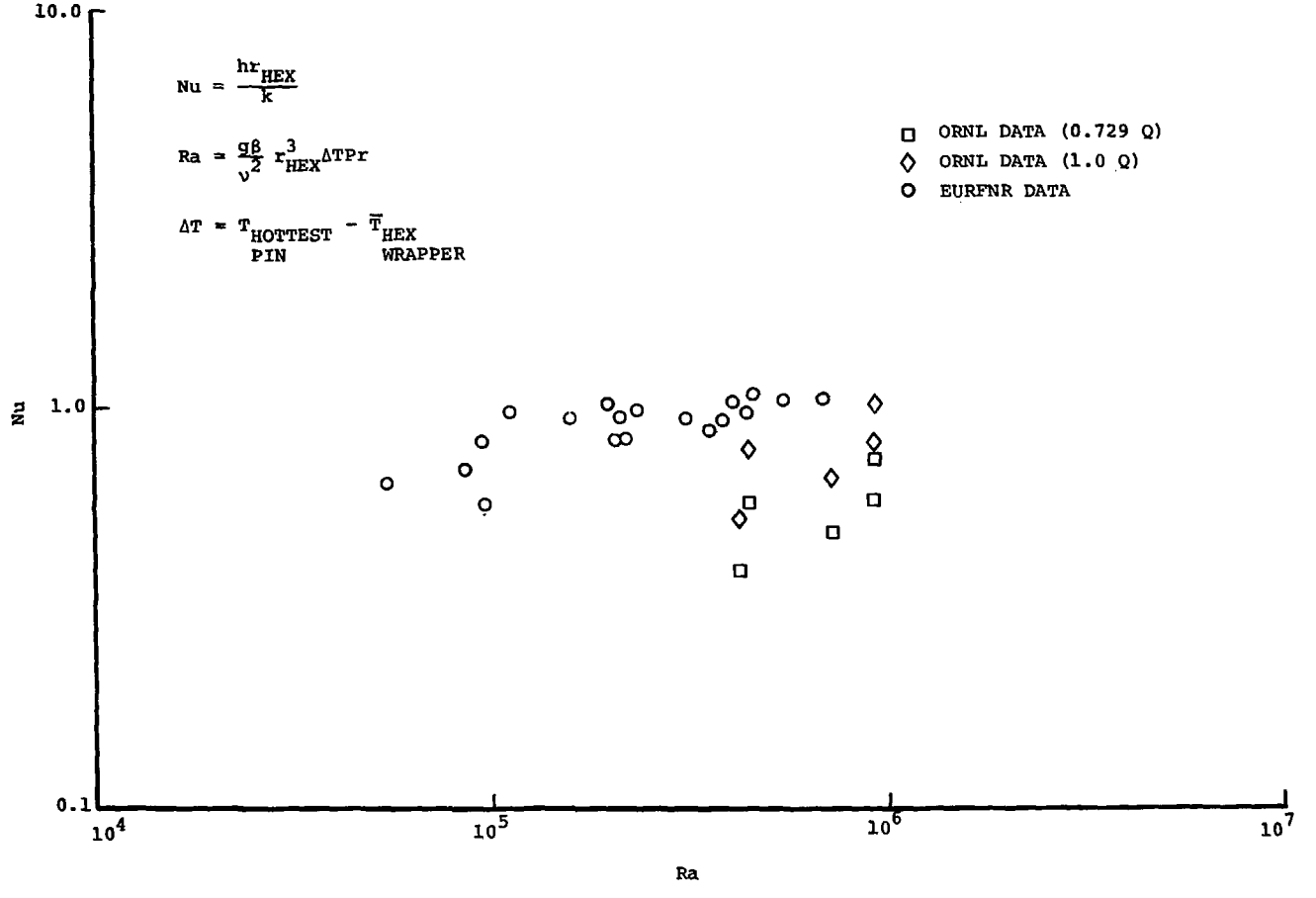

FIGURE 28. Nusselt Number Versus Rayleigh Number for a Sodium-Filled Hexagonal Fuel Pin Array

Option 3

1. Helium-filled basket
2. Sodium-filled canister

Option 4

1. Aluminum basket
2. Sodium-filled canister

For all four configurations, the helium pressure is assumed to be 5 atmospheres absolute. All emissivities on internal surfaces are 0.9. Copper fins ½ inch thick with a density of 10 fins/metre are used in the borated beechwood neutron shield. External fin density is 20 fins/metre.

Tables 1 through 4 are tabulations of the temperature increases of each section up to the hexagonal fuel array wrapper. Temperatures are in degrees Celsius. The first entry of 55 is the ambient temperature. The temperature increase for each cask section is entered in the table and added to the preceding temperature to find the section temperature.

The linear power densities at the top are "effective" quantities. In order to convert these to nominal values,* two more factors must be considered. The source spreading factor is an indicator of the extent to which the heat from the fuel pins is spread in the axial direction while still within the canister. Its value is equal to the inverse of the fraction of the heat which is transferred radially. Reference 3 states that, for assemblies packaged in helium, about 70% of the heat is transferred radially. This yields a source spreading factor (SSF) of 1.43.

The peaking factor is a coefficient which describes the power gradient in the heated section. If an assembly is said to have a peaking factor of 1.2 (a commonly used value), this indicates that its peak linear power density is 1.2 times its nominal linear power density.

*Nominal is the value (kW/m of heated length) actually assumed for fuel assemblies.

OPTION 1

HELIUM-FILLED BASKET
HELIUM-FILLED CANISTER

CASK SECTION	EFFECTIVE LINEAR POWER DENSITY* ($\frac{kW/m}{Assembly}$)				
	0.5	1.0	1.5	2.0	2.5
Ambient Temperature	55	55	55	55	55
Surface	37	63	84	104	121
Outer Cask	92	118	139	159	176
Conduction	25	51	76	102	127
Pipe To Steel Inner Containment Wall	117	169	215	261	303
	58	87	112	127	136
	175	256	327	388	439
Canister to Pipe	26	38	45	48	51
	201	294	372	436	490
Hex to Canister	37	70	106	143	183
Temperature of Hexagonal Array Wrapper	238	364	478	579	673

*See page 53 for method to determine nominal (actual) linear power density.

TABLE 1

Temperature Increment and Temperature Level in Degrees C for Option 1

OPTION 2

ALUMINUM BASKET
HELIUM-FILLED CANISTER

CASK SECTION	EFFECTIVE LINEAR POWER DENSITY* $\left(\frac{kW/m}{Assembly}\right)$				
	0.5	1.0	1.5	2.0	2.5
	55	55	55	55	55
Surface	37	63	84	104	121
	92	118	139	159	176
Outer Cask Conduction	25	51	76	102	127
	117	169	215	261	303
Pipe To Steel Inner Containment Wall	4	8	12	16	20
	121	177	227	277	323
Canister to Pipe	30	47	60	66	71
	151	224	287	343	394
Hex to Canister	36	65	96	129	166
Temperature of Hexagonal Array Wrapper	187	289	383	472	560

*See page 53 for method to determine nominal (actual) linear power density.

TABLE 2

OPTION 3

HELIUM-FILLED BASKET
SODIUM-FILLED CANISTER

CASK SECTION	EFFECTIVE LINEAR POWER DENSITY* $\left(\frac{kW/m}{Assembly}\right)$				
	0.5	1.0	1.5	2.0	2.5
	55	55	55	55	55
Surface	37	63	84	104	121
	92	118	139	159	176
Outer Cask Conduction	25	51	76	102	127
	117	169	215	261	303
Pipe To Steel Inner Containment Wall	58	87	112	127	136
	175	256	327	388	439
Canister to Pipe	26	38	45	48	51
	201	294	372	436	490
Hex to Canister	0	1	1	1	2
Temperature of Hexagonal Array Wrapper	201	295	373	437	492

*See page 53 for method to determine nominal (actual) linear power density.

TABLE 3

OPTION 4

ALUMINUM BASKET
SODIUM-FILLED CANISTER

CASK SECTION	EFFECTIVE LINEAR POWER DENSITY* (kW/m Assembly)				
	0.5	1.0	1.5	2.0	2.5
	55	55	55	55	55
Surface	37	63	84	104	121
	92	118	139	159	176
Outer Cask Conduction	25	51	76	102	127
	117	169	215	261	303
Pipe To Steel Inner Containment Wall	4	8	12	16	20
	121	177	227	277	323
Canister to Pipe	30	47	60	66	71
	151	224	287	343	394
Hex to Canister	0	1	1	1	2
Temperature of Hexagonal Array Wrapper	151	225	288	344	396

*See page 53 for method to determine nominal (actual) linear power density.

TABLE 4

Following the description of the two coefficients, one may write,

$$Q_{NOMINAL} = \frac{(SSF)}{(PF)} Q_{EFF} \quad .$$

Using a source spreading factor of 1.43 and peaking factor of 1.2 for the helium-canistered options, one finds that the effective source densities of 0.5, 1.0, 1.5, 2.0 and 2.5 kW/m/Assembly convert to nominal values of 0.596, 1.192, 1.788, 2.383 and 2.979 kW/m/Assembly, respectively. Similarly, using a source spreading factor of 3.0 and a peaking factor of 1.2 for sodium-canistered options, the nominal source densities become 1.25, 2.50, 3.75, 5.0 and 6.25 kW/m/Assembly, respectively.

Heat Transfer from Fuel Pins to Hexagonal Array Wrapper

A. Helium-Filled Canister

Governing Equations

$$\Delta T = 50\ M^{.31} Q_{PEAK}^{.63} \quad , \qquad \text{(Ref. 3)}$$

where,

M = the molecular weight of the gaseous coolant,

Q_{PEAK} = the peak linear source density in kW/m,

$$Q_{PEAK} = (PF)(Q_{NOM}) \quad .$$

For helium (M = 4) and using a peaking factor of 1.2, the equation reduces to,

$$\Delta T = 86.2\ Q_{NOM}^{.63} \quad .$$

Solution

Q_{NOM} (kW/m/Assembly)	ΔT (^{o}C)
0.596	62
1.192	96
1.788	124
2.383	149
2.974	171

B. Sodium-Filled Canister

Assumptions

For lack of a good correlation, let Nu = 0.3 (Section VII) where,

$$Nu = \frac{hr_{HEX}}{k} \quad .$$

Governing Equations

(SOURCE POWER) = (HEAT TRANSFER COEFFICIENT)(HEX AREA)
(*MAXIMUM PIN TEMPERATURE - HEX WRAPPER TEMPERATURE*)

$$Q_{PEAK} = hPer_{HEX}(T_{MAX\ PIN} - T_{HEX}) \quad ,$$

$$Per_{HEX} \approx 6.928\ r_{HEX} \quad ,$$

$$k_{Na} \approx 67\ W/m^{o}C\ @\ 500^{o}C \quad .$$

Solution

$$T_{MAX\ PIN} - T_{HEX} \approx 7.2^{o}C/kW/m \quad .$$

Q_{NOM} (P.F = 1.2) (kW/m/Assembly)	ΔT (^{o}C)
1.25	11
2.50	22
3.75	32
5.00	43
6.25	54

COMPARISON OF OPTIONS

At this point, a comparison between the options can be made. Tables 5 and 6 contain the results of the sections "Computation of Hexagonal Array Wrapper Temperature" and "Heat Transfer from Fuel Pins to Hexagonal Array Wrapper" and their sum, which is the maximum pin temperature for each option at the indicated nominal load. Figure 29 is a graph of these results. The horizontal line at 538^{o}C is the maximum allowable pin temperature. The intersection of this line and the predicted temperature curve indicates the maximum allowable nominal linear power density for each option when nine assemblies are to be shipped. These maximum allowable sources are 1.5, 1.9, 6.1 and 8.0 kW/m/Assembly for Options 1 through 4, respectively (see Table 7).

CONCLUSIONS

In order to analyze the heat transfer associated with the proposed shipping cask, the problem was divided into seven parts. The use of helium, liquid sodium and aluminum are considered as options to increase heat transfer efficiency where applicable. Ancillary problems of pipe material and thickness and liquid sodium correlations were considered. Predictions of maximum pin temperatures for several cask options were then calculated. Results of the calculations are shown in Table 7. Certain generalizations may be drawn from these predictions:

TEMPERATURE OF HOTTEST PIN
FOR FOUR OPTIONS

		$Q_{NOMINAL}$ (kW/m/Assembly)				
		0.596	1.192	1.788	2.383	2.979
OPTION 1	Hex Temp	238	364	478	579	673
	Hex-Pin ΔT	62	96	124	149	171
	Max Pin Temp	300	460	602	728	844
OPTION 2	Hex Temp	187	289	383	472	560
	Hex-Pin ΔT	62	96	124	149	171
	Max Pin Temp	249	385	507	621	731

Helium-Canistered Options
TABLE 5

		$Q_{NOMINAL}$ (kW/m/Assembly)				
		1.25	2.50	3.75	5.00	6.25
OPTION 3	Hex Temp	201	295	373	437	492
	Hex-Pin ΔT	11	22	32	43	54
	Max Pin Temp	212	317	405	480	546
OPTION 4	Hex Temp	151	225	288	344	396
	Hex-Pin ΔT	11	22	32	43	54
	Max Pin Temp	162	247	320	387	450

Sodium Canistered Options

TABLE 6

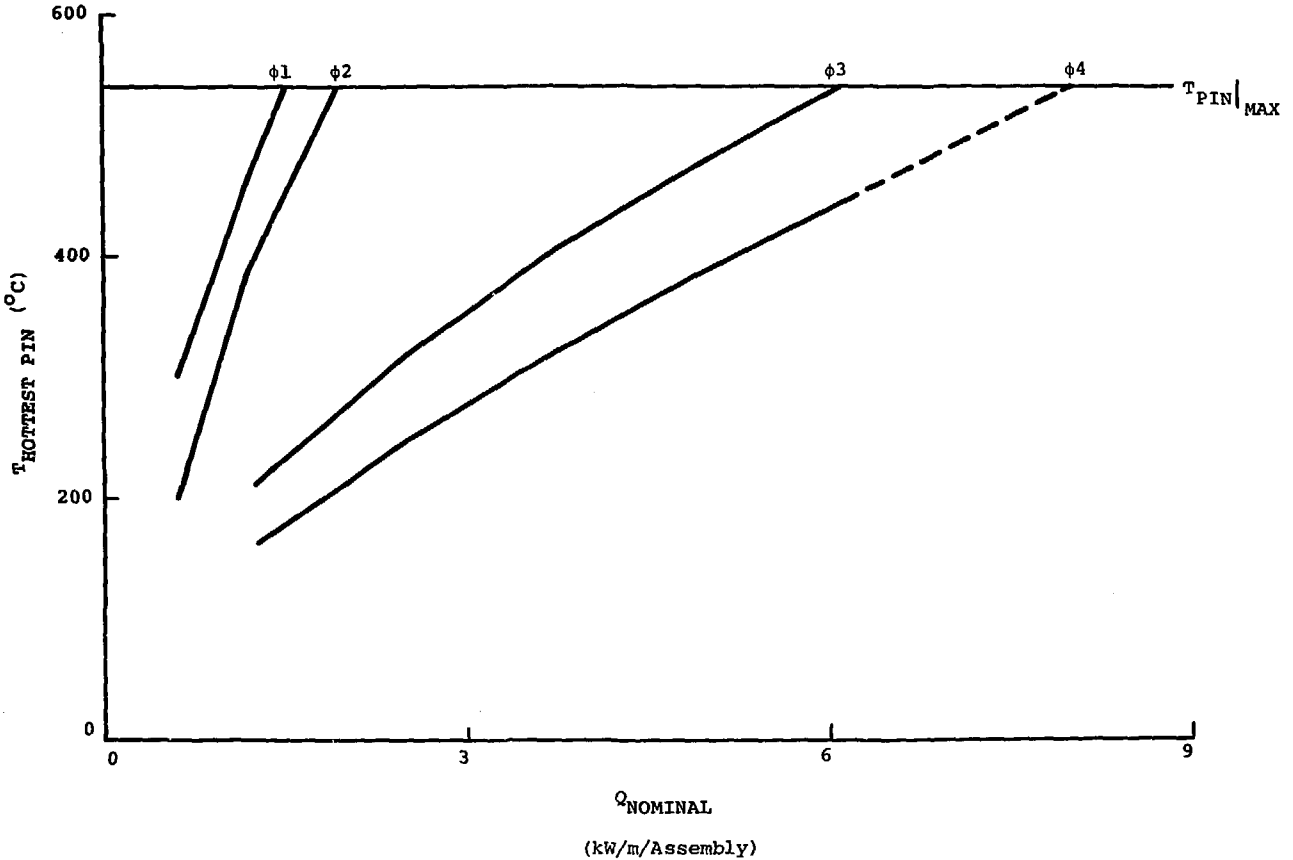

FIGURE 29. Hottest Pin Temperature Versus Axial Power Density for Four Cask Options

MAXIMUM NOMINAL LINEAR POWER
DENSITIES FOR FOUR CASK OPTIONS

CASK OPTION	MAXIMUM NOMINAL SOURCE STRENGTH (kW/m/Assembly)
Helium-Filled Basket Helium-Filled Canister	1.5
Aluminum Basket Helium-Filled Canister	1.9
Helium-Filled Basket Sodium-Filled Canister	6.1
Aluminum Basket Sodium-Filled Canister	8.0

TABLE 7

(1) The use of sodium in the canister increases dramatically the capacity of the cask. Source strengths about four times greater than possible with helium may be transported when sodium is used. Note: Where liquid sodium use was assumed, the calculations involving heat source spreading are felt to be conservative. The temperature spreading effects of liquid sodium are well documented in both the ORNL and the EURFNR reports. The source spreading factor for helium is far more uncertain.

(2) The use of an aluminum basket results in about a 30% increase in heat carrying capacity.

(3) The use of a selective surface on the outside of the cask provides a relatively small decrease in the surface temperature.

(4) It is important to use high emissivity surfaces in all cask cavities.

(5) If a helium-filled basket is to be used, the pipes should be made of either aluminum having a minimum wall thickness of 0.02 m or copper having a minimum wall thickness of 0.01 m.

At this point, it is appropriate to comment on the accuracy of the calculations. Certain relationships used in the predictions have a high degree of uncertainty associated with them. In particular, the heat transfer from pipe to gamma shield through the helium-filled basket should be considered only as a gross estimate with a high probable error. In general, all internal convective relationships involving gases need further investigation. On the other hand, the relationships involving the use of aluminum and liquid sodium result in far more accurate predictions of total carrying capacity. This is not to say that the relationships themselves are more accurate; rather that the uncertainties involved in these relationships impact the total capacity of the cask far less than those that involve gases.

Finally, it should be noted that these calculations are an attempt to est mate cask capacity and are not a prediction of actual temperature distribution The complexity of the heat transfer mechanisms prevents such predictions from being highly accurate. It is, therefore, recommended that tests be run using full scale model of the entire cask to provide detailed knowledge of temperatu distributions on a specific design.

SUMMARY

(1) Heat carrying capacity can be increased by 300% if assemblies are packaged in liquid sodium instead of helium.

(2) Heat carrying capacity can be increased by 30% if an aluminum basket is used in place of a helium-filled basket.

(3) The effect of using a selective surface on the outside of the cask is relatively small.

(4) All internal surfaces should have a high emissivity.

(5) If a helium-filled basket is to be used, pipes should be either 0.02 wall aluminum or 0.01 m wall copper.

(6) Further investigation of convective relationships is advised wherever gases are to be used.

(7) If knowledge of cask temperature distributions is deemed necessary, experiments should be run on a model of the entire cask.

REFERENCES

- L. B. Shappert, et al., "Cask Designers Guide," ORNL-NSIC-68, 1970.
- G. C. Allen, Jr., R. G. Eakes, J. M. Freedman, R. B. Pope, S. A. Dupree and W. P. Schimmel, Jr., "Conceptual Designs for LMFBR Shipping Casks," SAND77-1483, Sandia Laboratories, Albuquerque, NM, March 1978.
- R. B. Pope, "Evaluation of Heat Transfer for the Conceptual Designs of Spent Fuel Shipping Casks for the United States Fast Breeder Reactor Program," Sandia Laboratories, Albuquerque, NM, SAND77-1781, May 1978.
- W. M. Kays and A. L. London, Compact Heat Exchangers, McGraw-Hill Book Company, New York, 1964.
- Frank Kreith, Principles of Heat Transfer, Intext Press Inc., New York, 1973.
- R. B. Pope, Memo to Distribution, dtd 3/18/77, subject: A Potential Low Cost Neutron Shield for Shipping Casks.
- T. H. Kuehn and R. J. Goldstein, "Correlating Equations for Natural Convection Heat Transfer Between Horizontal Circular Cylinders," International Journal of Heat and Mass Transfer, Vol. 19, 1976, pp. 1127-1134.
- D. R. Lewis, et al., Chrysler Improved Numerical Differencing Analyzer for 3rd Generation Computers, TN-AP-67-287, Chrysler Corporation Space Division, New Orleans, LA, 1967.
- B. B. Klima, "LMFBR Spent Fuel Transport: Single-Assembly Heat Transport Test," ORNL-TM-4936, Oak Ridge National Laboratory, 1975.
- M. Prussman, B. Rappel and E. Weinert, "Heat Removal Experiments on an SNR Fuel Element Using a Sodium Filled Transport Container," Report No. KFK 2174, EURFNR-1301, Nuclear Energy Research Center Karlsruhe, Department of Reactor Operations and Technology, Fast Breeder Project (PSB), 1975.